(12) INTERNATIONAL APPLICATION PUBLISHED UNDER THE PATENT COOPERATION TREATY (PCT)

(19) World Intellectual Property Organization
International Bureau

(43) International Publication Date
10 October 2013 (10.10.2013)

(10) International Publication Number
WO 2013/152132 A1

(51) International Patent Classification:
H01L 31/042 (2006.01) *H01L 31/18* (2006.01)

(21) International Application Number:
PCT/US2013/035171

(22) International Filing Date:
3 April 2013 (03.04.2013)

(25) Filing Language: English

(26) Publication Language: English

(30) Priority Data:
61/619,661 3 April 2012 (03.04.2012) US
61/621,819 9 April 2012 (09.04.2012) US

(71) Applicant: **THE CALIFORNIA INSTITUTE OF TECHNOLOGY** [US/US]; 1200 E. California Boulevard, M/C 6-32, Pasadena, CA 91125 (US).

(72) Inventors: **ARDO, Shane**; 837 Magnolia Avenue #12, Pasadena, CA 91106 (US). **SHANER, Matthew**; 250 Machado Lane, San Luis Obispo, CA 93401 (US). **CORDAN, Robert**; 275 S. Marengo Avenue, #12, Pasadena, CA 91101 (US). **STRANDWITZ, Nicholas, C.**; 225 California Avenue, Santa Monica, CA 90403 (US). **MCKONE, James, R.**; 344 South Allen Avenue, Pasadena, CA 91106 (US). **FOUNTAINE, Katherine**; 366 S. Catalina Avenue, #301, Pasadena, CA 91106 (US). **ATWATER, Harry, A.**; 1945 Leman Street, S. Pasadena, CA 91030 (US). **LEWIS, Nathan, S.**; 4808 Gould Avenue, La Canada Flintridge, CA 91011 (US).

(74) Agent: **BAKER, Joseph, R.**; Gavrilovich, Dodd & Lindsey LLP, 4660 La Jolla Village Drive, Suite 750, San Diego, CA 92122 (US).

(81) Designated States *(unless otherwise indicated, for every kind of national protection available)*: AE, AG, AL, AM, AO, AT, AU, AZ, BA, BB, BG, BH, BN, BR, BW, BY, BZ, CA, CH, CL, CN, CO, CR, CU, CZ, DE, DK, DM, DO, DZ, EC, EE, EG, ES, FI, GB, GD, GE, GH, GM, GT, HN, HR, HU, ID, IL, IN, IS, JP, KE, KG, KM, KN, KP, KR, KZ, LA, LC, LK, LR, LS, LT, LU, LY, MA, MD, ME, MG, MK, MN, MW, MX, MY, MZ, NA, NG, NI, NO, NZ, OM, PA, PE, PG, PH, PL, PT, QA, RO, RS, RU, RW, SC, SD, SE, SG, SK, SL, SM, ST, SV, SY, TH, TJ, TM, TN, TR, TT, TZ, UA, UG, US, UZ, VC, VN, ZA, ZM, ZW.

(84) Designated States *(unless otherwise indicated, for every kind of regional protection available)*: ARIPO (BW, GH, GM, KE, LR, LS, MW, MZ, NA, RW, SD, SL, SZ, TZ, UG, ZM, ZW), Eurasian (AM, AZ, BY, KG, KZ, RU, TJ, TM), European (AL, AT, BE, BG, CH, CY, CZ, DE, DK, EE, ES, FI, FR, GB, GR, HR, HU, IE, IS, IT, LT, LU, LV, MC, MK, MT, NL, NO, PL, PT, RO, RS, SE, SI, SK, SM, TR), OAPI (BF, BJ, CF, CG, CI, CM, GA, GN, GQ, GW, ML, MR, NE, SN, TD, TG).

Published:
— *with international search report (Art. 21(3))*

(54) Title: SEMICONDUCTOR STRUCTURES FOR FUEL GENERATION

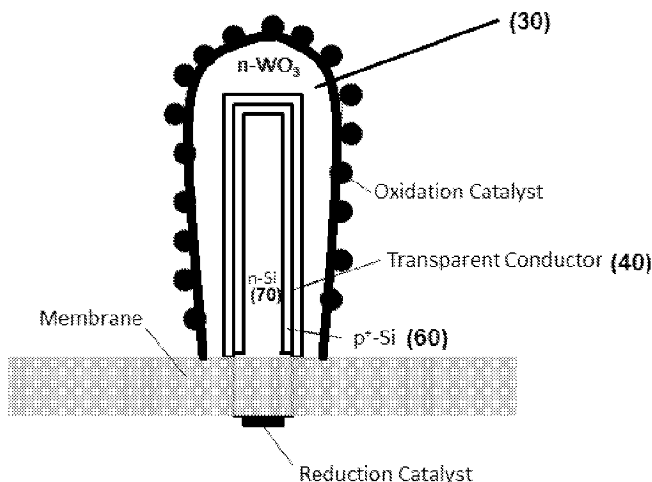

FIGURE 11A

(57) Abstract: This disclosure relates to photovoltaic and photoelectrosynthetic cells, devices, and methods of making by using an elongated structure comprising a plurality of radially-integrated tandem junctions separated by a transparent low resistance layer, wherein a first junction comprising a first semi conductive material and at least a second junction comprising a second different or the same semiconducting material having a different or the same band gap compared to the first semi conductive material.

WO 2013/152132 A1

SEMICONDUCTOR STRUCTURES FOR FUEL GENERATION

CROSS REFERENCE TO RELATED APPLICATIONS

[0001] This application claims priority to U.S. Provisional Application Serial No. 61/619,661, filed April 3, 2012 and U.S. Provisional Application No. 61/621,819, filed April 9, 2012, the disclosures of which are incorporated herein by reference.

STATEMENT REGARDING FEDERALLY SPONSORED RESEARCH

[0002] This invention was made with government support under Grant No. DE-SC0004993 awarded by the Department of Energy (JCAP). The government has certain rights in the invention.

TECHNICAL FIELD

[0003] This invention relates to photovoltaic cells, devices, water splitting devices and methods of making and using the same.

BACKGROUND

[0004] Ordered arrays of crystalline-Si (c-Si) microwires, fabricated by chemical-vapor-deposition, vapor–liquid–solid (CVD-VLS) growth mechanism, were pioneered nearly five years ago for sunlight-to-electrical power conversion. P-type Si microwire arrays, employing a thin n^+-doped emitter layer to form a buried junction (p-n^+-Si), have since realized sunlight-to-electrical power-conversion efficiencies > 7% from solid-state photovoltaic (PV) devices, and > 5% power-conversion efficiency toward H_2 evolution from acidic aqueous electrolytes when functionalized with Pt electrocatalysts. In the absence of additional processing-intensive steps for light absorption enhancement, these devices demonstrated a short-circuit (maximum) current density (j_{sc}) ≈ 9 mA/cm^2, open-circuit (maximum) photovoltage (V_{oc}) ≈ 0.53 V, and fill factor ≈ 70%. The product of these three terms determines the power-conversion efficiency of the device. The Si microwire geometry uses ~5% of the material required for conventional wafer-based photovoltaics (PVs) and absorbs ~20% of above bandgap sunlight. Various designs to alter the path of light and increase absorption by the Si microwire arrays, and thus j_{sc} and the efficiency, have been investigated with modest success.

[0005] Si microwire array photocathodes have been shown to generate photovoltages in excess of 500 mV in acidic aqueous environments, and provide a desirable geometry, relative to planar structures, for devices that effect the unassisted generation of fuels from sunlight. Microwire arrays benefit from orthogonalization of the directions of light absorption and minority-carrier collection, as well as from light-trapping effects, an increased surface area for catalyst loading per unit of geometric area, a small solution resistance as compared to planar designs, a reduced material usage through reusable substrates; and from the ability to embed the microwires into ion exchange membranes that exhibit little permeability to H_2 and O_2, thereby producing flexible devices that persistently separate the products of the water-splitting reaction.

[0006] However, the voltage generated from single-junction Si microwire arrays is much lower than the 1.23 V required for solar-driven water splitting.

SUMMARY

[0007] The disclosure provides an elongated structure comprising a plurality of radially-integrated tandem junctions separated by a transparent low resistance layer, wherein a first junction comprises a first semiconductive material and at least a second junction comprises a second different or the same semiconducting material having a different or the same band gap compared to the first semiconductive material. In one embodiment, the first junction and second junction are separated by a low resistance layer comprising a transparent conductive oxide. In one embodiment, the low resistance layer comprises one or more of a material selected from the group consisting of TiO_2, $CaTiO_3$, $SrTiO_3$, $Sr_3Ti_2O_7$, $Sr_4Ti_3O_{10}$, $Rb_2La_2Ti_3O_{10}$, $Cs_2La_2Ti_3O_{10}$, $CsLa_2Ti_2NbO_{10}$, La_2TiO_5, $La_2Ti_3O_9$, $La_2Ti_2O_7$, $La_2Ti_2O_7$:Ba, $KaLaZr_{0.3}Ti_{0.7}O_4$, $La_4CaTi_5O_{17}$, $KTiNbO_5$, $Na_2Ti_6O_{13}$, $BaTi_4O_9$, $Gd_2Ti_2O_7$, $Y_2Ti_2O_7$, ZrO_2, $K_4Nb_6O_{17}$, $Rb_4Nb_6O_{17}$, $Ca_2Nb_2O_7$, $Sr_2Nb_2O_7$, $Ba_5Nb_4O_{15}$, $NaCa_2Nb_3O_{10}$, $ZnNb_2O_6$, $Cs_2Nb_4O_{11}$, La_3NbO_7, Ta_2O_5, $KsPrTa_5O_{15}$, $K_3Ta_3Si_2O_{13}$, $K_3Ta_3B_2O_{12}$, $LiTaO_3$, $KTaO_3$, $AgTaO_3$, $KTaO_3$:Zr, $NaTaO_3$:La, $NaTaO_3$:Sr, $Na_2Ta_2O_6$, $CaTa_2O_6$, $SrTa_2O_6$, $NiTa_2O_6$, $Rb_4Ta_6O_{17}$, $Ca_2Ta_2O_7$, $Sr_2Ta_2O_7$. $K_2SrTa_2O_7$, $RbNdTa_2O_7$, $H_2La_{2/3}Ta_2O_7$, $K_2Sr_{1.5}Ta_3O_{10}$, $LiCa_2Ta_3O_{10}$, $KBa_2Ta_3O_{10}$, $Sr_5Ta_4O_{15}$, $Ba_2Ta_4O_{15}$, $H_{1.8}Sr_{0.81}Bi_{0.19}Ta_2O_7$, Mg—Ta Oxide, $LaTaO_4$, $LaTaO_7$, $PbWO_4$,

$RbWNbO_6$, $RbWTaO_6$, CeO_2:Sr, $BaCeO_3$, $NaInO_2$, $CaIn_2O_4$, $SrIn_2O_4$, $LaInO_3$, $Y_xIn_{2-x}O_3$, $NaSbO_3$, $CaSb_2O_6$, $Ca_2Sb_2O_7$, $Sr_2Sb_2O_7$, Sr_2SnO_4, $ZnGa_2O_4$, Zn_2GeO_4, $LiInGeO_4$, $Ga_2O_3^b$, Ga_2O_3:Zn^c, $Na_2Ti_3O_7$, $K_2Ti_2O_5$, $K_2Ti_4O_9$, $Cs_2Ti_2O_5$, H^+-$Cs_2Ti_2O_5$, $Cs_2Ti_5O_{11}$, $Cs_2Ti_6O_{13}$, H^+-$CsTiNbO_5$, H^+-$CsTi_2NbO_7$, SiO_2-pillared $K_2Ti_4O_9$, SiO_2-pillared $K_2Ti_{2.7}Mn_{0.3}O_7$, $Na_2W_4O_{13}$, H^+-$KLaNb_2O_7$, H^+-$RbLaNb_2O_7$, H^+-$CsLaNb_2O_7$, H^+-$KCa_2Nb_3O_{10}$, SiO_2-pillared $KCa_2Nb_3O_{10}$, ex-$Ca_2Nb_3O_{10}/K^+$ nanosheet[4)], Restacked ex-$Ca_2Nb_3O_{10}/Na^+$, H^+-$RbCa_2Nb_3O_{10}$, H^+-$CsCa_2Nb_3O_{10}$, H^+-$KSr_2Nb_3O_{10}$, H^+-$KCa_2NaNb_4O_{13}$, $Bi_2W_2O_9$, $Bi_2Mo_2O_9$, $Bi_4Ti_3O_{12}$, $BaBi_4Ti_4O_{15}$, Bi_3TiNbO_9, $PbMoO_4$, $(NaBi)_{0.5}MoO_4$, $(AgBi)_{0.5}MoO_4$, $(NaBi)_{0.5}WO_4$, $(AgBi)_{0.5}WO_4$, $Ga_{1.14}In_{0.86}O_3$, β-Ga_2O_3, $Ti_{1.5}Zr_{1.5}(PO_4)_4$, WO_3, Bi_2WO_6, Bi_2MoO_6, $Bi_2Mo_3O_{12}$, $Zn_3V_2O_8$, $Na_{0.5}Bi_{1.5}VMoO_8$, $In_2O_3(ZnO)_3$, $SrTiO_3$:Cr/Sb, $SrTiO_3$:Ni/Ta, $SrTiO_3$:Cr/Ta, $SrTiO_3$:Rh, $CaTiO_3$:Rh, $La_2Ti_2O_7$:Cr, $La_2Ti_2O_7$:Fe, TiO_2:Cr/Sb, TiO_2:Ni/Nb, TiO_2:Rh/Sb, $PbMoO_4$:Cr, $RbPb_2Nb_3O_{10}$, $PbBi_2Nb_2O_9$, $BiVO_4$, $BiCu_2VO_6$, $BiZn_2VO_6$, $SnNb_2O_6$, $AgNbO_3$, Ag_3VO_4, $AgLi_{1/3}Ti_{2/3}O_2$, $AgLi_{1/3}Sn_{2/3}O_2$, $LaTiO_2N$, $Ca_{0.25}La_{0.75}TiO_{2.25}N_{0.75}$, TaON, Ta_3N_5, $CaNbO_2N$, $CaTaO_2N$, $SrTaO_2N$, $BaTaO_2N$, $LaTaO_2N$, $Y_2Ta_2O_5N_2$, $TiN_xO_yF_z$, $Sm_2Ti_2O_5S_2$, La-In oxysulfide, GaAs, GaP, $GaAs_xP_{1-x}$, Al_xGa_{1-x}, As, $Al_xGa_{1-x}As_yP_{1-y}$, $In_xGa_{1-x}As$, $In_xGa_{1-x}P$, $In_xGa_{1-x}As_yP_{1-y}$, $Al_xIn_{1-x}As_yP_{1-y}$, $Al_xGa_{1-x}As_yN_zP_{1-y-z}$, $In_xGa_{1-x}As_yN_zP_{1-y-z}$, Zn_3P_2, Zn_3S_2, and ZnP_xS_{1-x} ($0\leq x\leq 1$, $0\leq y\leq 1$, $0\leq z\leq 1$, $0\leq y+z\leq 1$). In one embodiment, the second semiconductive layer comprises a material selected from the group consisting of GaAs, GaP, $GaAs_xP_{1-x}$, Al_xGa_{1-x}, As, $Al_xGa_{1-x}As_yP_{1-y}$, $In_xGa_{1-x}As$, $In_xGa_{1-x}P$, $In_xGa_{1-x}As_yP_{1-y}$, $Al_xIn_{1-x}As_yP_{1-y}$, $Al_xGa_{1-x}As_yN_zP_{1-y-z}$, $In_xGa_{1-x}As_yN_zP_{1-y-z}$, Zn_3P_2, Zn_3S_2, and ZnP_xS_{1-x} ($0\leq x\leq 1$, $0\leq y\leq 1$, $0\leq z\leq 1$, $0\leq y+z\leq 1$). In another embodiment, the low resistance layer comprises indium tin oxide (ITO). In yet another embodiment, the elongated structure has a dimension comprising 500 nm to about 10 micrometers in diameter and about 1 micrometer to 1 mm in length or wherein the elongated structure has a mean diameter less than 1 micrometer and a length of less than 1 micrometer and an aspect ratio of greater than 1. In yet another embodiment, the elongated structure has an aspect ratio greater than 1. In one embodiment, the first semiconductive material is Si. In another embodiment, the elongated structure is substantially embedded in a material selected from the group consisting of glass, polymer and wax. In yet a further embodiment, the material forms a membrane comprising the elongated structure embedded in the material extending from and/or through a first

surface to and/or through a second surface of the membrane. In one embodiment, one or both ends of the elongated structure are coated with a catalyst. In yet another embodiment, the first conductive material and/or the second conductive material are designed geometrically to optimize light incidence or collection at one or both of the materials. In a further embodiment, the tops of the elongated structures are flat. In yet another embodiment, the first semiconductive layer comprises a material selected from the group consisting of crystalline Si, multicrystalline Si, GaAs, InP, CdTe and alloys of any of the foregoing, or group IV metal dichalcogenides; the low resistance layer comprise a material selected from the group consisting of ITO (In-SnO_2), FTO (F-doped SnO_2), and TiO_2; and the second semiconductive layer comprises a material selected from the group consisting of WO_3, BiVO4, Fe_2O_3, GaP, CdSe, and amorphous-Si. In a further embodiment, the group IV metal dicholcogenides is selected from the group consisting of MoS_2, WS_2, $MoSe_2$, and WSe_2.

[0008] The disclosure also provides a method of making the structures descrbied above, comprising: (a) fabricating a first semiconductive structures on a Si substrate comprising (i) forming a templated oxide layer on the substrate, wherein the template for the templated oxide layer comprises openings in the oxide layer for the formation of a first semiconductive structure; and (ii) growing a set of first semiconductive structures on the substrate, wherein the first semiconductive structure growth is supported by a catalyst deposited in the openings in the oxide layer; (b) coating the fabricated first semiconductive structures in an oppositely doped semiconductive material layer to generate an emitter layer; (c) coating the emitter layer with an transparent low resistance layer; and (d) radially and epitaxially applying a second semiconductive material on the transparent low resistance layer, wherein the second semiconductive material has the same or wider band-gap as the first semiconductive material. In one embodiment, the low resistance layer comprises a semiconductive material. In another embodiment, the low resistance layer comprises a transparent conductive oxide. In yet another embodiment, the transparent conductive oxide is

selected from the group consisting of cadmium tin oxide (CTO), indium tin oxide (ITO), fluorine-doped tin oxide (SnO:F or FTO), indium-doped cadmium-oxide, cadmium stannate (Cd_2SnO_4 or CTO), doped zinc oxide (ZnO), such as aluminum-doped zinc-oxide (ZnO:Al or AZO), indium-zinc oxide (IZO), zinc tin oxide ($ZnSnO_x$), and combinations thereof. In yet another embodiment, the elongated structure is substantially embedded in a wax, glass or polymer. In yet another embodiment, the embedded elongated structure are mechanically removed from the Si substrate. In still another embodiment, the method further comprises applying a hydrogen evolving and/or oxygen evolving catalyst to the elongated structure. In a further embodiment, the catalyst is selected from the group consisting of Pt, Co, Cu, Fe, MoS_x where x is nominally 2, or a sub or super-stoichiometric, Ni, CoMo, CoW, FeMo, NiCo, NiFe, NiFeC, NiFeS, NiMnS, NiMo, NiMoP, NiSn, NiW, NiZn, NiZnP, CoNiFe, NiCoPMo, NiMoCo, NiMoCu, NiMoFe, NiMoW, NiSiMo, NiSiW, NiWPCu, IrO_x where x is nominally 2, or sub or super-stoichiometric, Pt, Co, Co/$(PO_4)^{3-}$, Co/$(BO_3)^{3-}$, CoP, Cu, Fe, Mn, Ni, Ni/$(BO_3)^{3-}$,NiP, Pb, CoFe, $CoPSc_2O_3$, FeMn, NiCo, NiCr, NiCu, NiFe, NiLa, NiLa, $NiPSc_2O_3$, NiSn, NiZn and NiMoFe.

[0009] The disclosure also provides a solar cell or photoelectrosynthetic device comprising the structure of any embodiment described herein. In one embodiment, the device comprises: a substrate; an ordered array of elongate semiconductor structures comprising at least 2 different semiconductive materials axially and radially integrated, wherein the elongate semiconductor structures have length dimensions defined by adjacent ends in electrical contact with at least portions of the substrate and distal ends not in contact with the substrate and have radial dimensions generally normal to the length dimensions and the radial dimensions are less than the length dimensions; a transparent low resistive layer separating the at least 2 different semiconductive materials; and wherein the device absorbs received light and converts it into electricity or chemical energy. In one embodiment, the elongated semiconductor structures comprise wires. In another embodiment, the elongate semiconductor structures are

embedded in a matrix. In yet another embodiment, the matrix is a glass, polymer or wax. In yet a further embodiment, the elongate semiconductor structures are partially or fully embedded in a matrix.

BRIEF DESCRIPTION OF THE DRAWINGS

[0010] **Figure 1A-F** shows a device schematic of the disclosure. (a) shows a schematic of a single tandem junction wire of the disclosure. (b) shows another schematic of a single tandem junction wire of the disclosure and includes a membrane and OER and HER catalysts. (c) Tandem junction microwire array with a buried, homo-junction (n-p^+-Si) coated by ITO and n-WO_3. (d) 2D cross-section of an individual tandem junction array unit cell. (e) Electronic structure of tandem device in the dark showing the buried n-p^+-Si junction, ohmic Si/ITO/n-WO_3 junction, and n-WO_3/liquid junction. The device is shown equilibrated with the oxygen evolution potential. (f) Steady-state electronic structure of tandem device under illumination with carrier movement directions shown. Both the oxygen and hydrogen evolution potentials are shown with the overpotentials accounted for by the difference between the respective quasi-Fermi level and reaction potential. Electrons and holes are collected radially in the n-WO_3. Holes are collected radially in the n-p^+-Si and electrons are collected axially at the back contact.

[0011] **Figure 2A-F** shows a tandem junction fabrication method of the disclosure. (a) photolithographically patterned n^+-Si <111> wafer with a SiO_2 mask layer and Cu catalyst in the desired growth pattern. (b) VLS Cu-catalyzed growth of n-type Si microwires on n^+-Si substrate followed by a metal etch (RCA 2). (c) SiO_2 reaction barrier (boot) formation via SiO_2 growth, partial polydimethylsiloxane (PDMS) infill, HF etch and PDMS removal. (d) p^+-Si emitter drive-in from BCl_3 precursor at 950°C for 30min in a CVD furnace. (e) Conformal DC sputter coating of ITO. (f) Conformal n-WO_3 electrodeposition and annealing at 400°C for 2h.

[0012] **Figure 3A-C** shows non-aqueous n-p^+-Si buried junction performance. (a) Non-aqueous PEC (forward scan, scan rate = 20 $mV\text{-}s^{-1}$) results using ferrocene$^{+/0}$ (black) and cobaltocene$^{+/0}$ (blue) as

redox couples to probe the n-p^+-Si buried junction performance in microwires arrays. The dark scans are dashed lines and light scans are shown as solid lines. (b) SEM image near the base of the Si microwire devices that displays the SiO_2 boot. (c) Redox potentials of cobaltocene ($(Cp)_2Co^{+/0}$) and ferrocene ($(Cp)_2Fe^{+/0}$) with respect to the potentials of the conduction band edge and the valence band edge of Si.

[0013] **Figure 4A-C** shows aqueous single (WO_3/liquid junction) and tandem junction device performance. (a) Three electrode PEC (forward scan, scan rate = 20 mV-s^{-1}) performance for single (blue) and tandem (black) junction microwire devices in contact with 1.0 M H_2SO_4(aq). The single junction microwire device consisted of WO_3 supported on p-Si microwires that had been coated with ITO. Here the p-Si/ITO contact is ohmic so the only rectifying junction is at the WO_3/liquid junction. These data demonstrate the presence of an additive voltage from each junction, with 0.73 V and 0.5 V produced by the WO_3/liquid and n-p^+-Si buried junctions, respectively. The V_{oc} for the single junction device was defined as the point at which the dark current, due to capacitive charging, and the illuminated current separated. The V_{oc} for the tandem junction device was defined as the point at which no current was flowing because no positive dark current existed in this region. (b) SEM image of p-Si/ITO/WO_3 single junction microwire devices. (c) SEM image of tandem junction devices.

[0014] **Figure 5A-B** shows load-line analysis and two electrode performance. (a) *J–E* curves and load-line analysis of the tandem junction (n-p^+-Si/ITO/WO_3) microwire device at 11 suns plotted against the dark HER curves (mirrored about the abscissa) using a Pt disc electrode in an Ar(g)- or H_2(g)-saturated solution. These measurements were conducted in a two-electrode cell with 1 M H_2SO_4 in both compartments separated by a Nafion® membrane to maintain product separation. The Pt disc HER curves include solution and membrane resistances because the reference electrode (SCE) was placed in the opposite cell at the same location used for the tandem microwire array device. The inset is a zoomed in view around the operational points, which are indicated by the red (Ar) and blue

(H_2) circles. (b) Two-electrode measurements at 0 V applied bias between the tandem junction device (11 Suns illumination) and Pt disc electrode in either Ar(g)- or H_2(g)-saturated solution. Turning the light off, as indicated, demonstrated that the positive current was photoinduced.

[0015] **Figure 6A-B** shows modeled tandem junction performance. Modeled *J–E* curves and load-line analysis for unconcentrated (a) and concentrated (b) illumination conditions that match the experimental photon fluxes at 1 and 12 Suns. The Si homo-junction is shown with (green) and without (black) inclusion of realistic hydrogen evolution catalytic overpotentials. Butler–Volmer kinetics with α = 1 and $j_0 = 10^{-3}$ A-cm^{-2} was used to calculate the catalytic overpotentials in the absence of mass transport limitations. The insets show the operating point for unconcentrated illumination ((a) black dot) and for concentrated illumination, with ((b) green dot) and without ((b) black dot) overpotential due to HER catalysis included. The rate of catalysis is not expected to affect the WO_3 *J–E* behavior due to the large band gap of WO_3 and proximity of $E^{o\prime}(O_2/H_2O)$ to the potential of the conduction band of WO_3.

[0016] **Figure 7** shows a monolithic, microwire, tandem PEC device depicting a hydrogen evolution reaction (HER) catalyst, oxygen evolution reaction (OER) catalyst, ion-conducting membrane and a photoanode and photocathode separated by an ohmic contact; half reactions for water-splitting under acidic conditions are shown.

[0017] **Figure 8** shows Plot of Si, Al, and WO_3 absorption vs. wavelength, showing substantial absorption in the aluminum.

[0018] **Figure 9A-I** show nine diagrams of design modifications with an opaque contact, aiming to understand and decrease contact absorption losses; not to scale; A) elimination of the round top; B) elimination of the tapered sides; C) combination of A and B; D) convex-shaped WO_3 top; E) smaller radius in the top half of the wire; F) similar to E but with the WO_3 layer flush with the bottom half of the silicon wire; G) elimination of the top Al surface; H) pyramidal Al top surface; I) Rounded top of Si and Al.

[0019] **Figure 10** shows a plot of aluminum absorption vs. wavelength for a planar substrate and an Al coated Si wire.

[0020] **Figure 11A-E** shows devices of the disclosure. (A) shows a photoactive (not low resistance) junction can be a semiconductor-liquid junction (at n-WO_3 | solution.). The other junction is not a semiconductor-liquid junction (at n-Si and p^+-Si. The photoactive semiconductor regions (both labeled on the materials) are doped the same (*e.g.*, n-type in this embodiment). (B) Both photoactive junctions can be semiconductor-liquid junctions (at n-WO_3 | solution and p-Si solution). The photoactive semiconductor regions (both labeled on the materials) are doped opposite. The conductor could be non-transparent, especially if the p-Si is p^+-Si; if the top is p^+-Si, the conductor is non-transparent and highly reflective to bounce light around to the bottom p-Si; p^+-Si, with a reflective layer, is another embodiment and is included in the alternative designs. (C) A buried pn^+ junction can be formed at the bottom affording the largest voltages regardless of the catalyst work function. (D) The membrane is thicker for mechanical stability; the bottom junction is buried, however then the reduction catalyst can be a solid layer like in (A) (above). (E) The p^+-Si region is extremely thin (*e.g.*, about 10 to 100s of nanometers in diameter. In all of A-E the reflective conductor is also as thin as possible so that the incident light can more easily see the bottom Si. The H_2 evolution catalyst is a reductive catalyst, in general. The O_2 evolution catalyst is an oxidative catalyst, in general. The dopant configuration can be switched, but all doped regions are switched and the catalysts are switched.

DETAILED DESCRIPTION

[0021] As used herein and in the appended claims, the singular forms "a," "and," and "the" include plural referents unless the context clearly dictates otherwise. Thus, for example, reference to "a pillar" includes a plurality of such pillars and reference to "the catalyst" includes reference to one or more catalysts known to those skilled in the art, and so forth.

[0022] Also, the use of "or" means "and/or" unless stated otherwise. Similarly, "comprise," "comprises," "comprising" "include," "includes," and "including" are interchangeable and not intended to be limiting.

[0023] It is to be further understood that where descriptions of various embodiments use the term "comprising," those skilled in the art would understand that in some specific instances, an embodiment can be alternatively described using language "consisting essentially of" or "consisting of."

[0024] Unless defined otherwise, all technical and scientific terms used herein have the same meaning as commonly understood to one of ordinary skill in the art to which this disclosure belongs. Although methods and materials similar or equivalent to those described herein can be used in the practice of the disclosed methods and compositions, the exemplary methods, devices and materials are described herein.

[0025] The publications discussed above and throughout the text are provided solely for their disclosure prior to the filing date of the present application. Nothing herein is to be construed as an admission that the inventors are not entitled to antedate such disclosure by virtue of prior disclosure.

[0026] By "about" is meant a quantity, level, value, number, frequency, percentage, dimension, size, amount, weight or length that varies by as much as 30, 25, 20, 15, 10, 9, 8, 7, 6, 5, 4, 3, 2 or 1% to a reference quantity, level, value, number, frequency, percentage, dimension, size, amount, weight or length. With respect to ranges of values, the disclosure encompasses each intervening value between the upper and lower limits of the range to at least a tenth of the lower limit's unit, unless the context clearly indicates otherwise. Further, the invention encompasses any other stated intervening values. Moreover, the invention also encompasses ranges excluding either or both of the upper and lower limits of the range, unless specifically excluded from the stated range.

[0027] The term "array" generally refers to multiple numbers of structures distributed within an area and spaced apart, although possible touching in some places, unless otherwise indicated. Structures within an array all do not have to have the same orientation.

[0028] The term "aspect ratio" refers to the ratio of a structure's length to its width. Hence, the aspect ratios of the

elongate structures will be greater than one. In various embodiments, the diameter of, for example, a "rod" or "wire" is about 10-50 nm, about 50-100 nm, about 100-500 nm, about 500nm-1μm, about 1μm-10μm or about 10μ-100μm. Typically the diameter will be about 1-10μm. The length of the "rod" or "wire" is about 1μm-10μm, about 10μm-100μm, or about 100μm-several millimetres.

[0029] The terms "ball," "spheroid," "blob" and other similar terms may also be used synonymously, except as otherwise indicated. Generally, these terms refer to structures with the width defined by the longest axis of the structure and the length defined by the axis generally normal to the width. Hence, the aspect ratio of such structures will generally be unity or less than unity.

[0030] As used herein, "elongated structure" refers to a structure having an aspect ratio greater than 1 wherein the structure can be uniform or non-uniform along its axis. For example, the elongated structure can be conical, hour-glass, an inverted conical, and the like. The elongated structure has one axis that is longer than a perpendicular axis. The longer axis can be several to about 999 nm in length (*e.g.*, a nano-elongated structure), or may be a micron to 999 microns in length or longer (*e.g.*, micro-elongated structures).

[0031] The terms "ordered" or "well-defined" generally refer to the placement of elements in a specified or predetermined pattern where the elements have distinct spatial relationships to one another. Hence, the terms "ordered array" or "well-defined" generally refer to structures distributed within an area with distinct, specified or predetermined spatial relationships to one another. For example, the spatial relationships within an ordered array may be such that the structures are spaced apart from one another by generally equal distances. Other ordered arrays may use varying, but specified or predetermined, spacings. The structures within "ordered" or "well-defined" arrays may also have similar orientations with respect to each other.

[0032] A "photovoltaic cell" is an electrical device comprising a semiconductor that converts light or other radiant energy, in the range from ultraviolet to infrared radiation, incident on its

surface into electrical energy in the form of power/voltage/current and which has two electrodes, usually at least one diode where the diode has a top electrode and a bottom electrode with opposite electrical polarities. The photovoltaic cell produces direct current which flows through the electrodes. As employed herein, the term photovoltaic cell is generic to cells which convert radiant energy into electrical energy. A solar cell is a photocell that converts light including solar radiation incident on its surface into electrical energy.

[0033] A photovoltaic ("PV") cell may be connected in parallel, in series, or a combination thereof with other such cells. A common PV cell is a p-n junction device based on crystalline silicon. In various embodiments of the disclosure a PV cell comprises p-n junction devices of silicon elongated structure. In other embodiments a PV cell comprises a plurality of silicon p-n junctions. Other types of PV cells can be based on a p-n junction cell of silicon and other semiconductive materials, such as, but not limited to, amorphous silicon, polycrystalline silicon, germanium, organic materials, Group III-V semiconductor materials, such as gallium arsenide (GaAs), Group II-VI semiconductor materials, such as cadmium sulfide (CdS), metal oxides, nitrides, or chalcogenides, such as zinc oxide, and mixed ternary, and larger number component, materials.

[0034] During operation of a photovoltaic cell, incident solar or light radiation penetrates below a surface of the PV cell and is absorbed. The depth at which the solar radiation penetrates depends upon an absorption coefficient of the cell. In the case of a PV cell based on silicon, an absorption coefficient of silicon varies with wavelength of solar radiation. At a particular depth within the PV cell, absorption of solar radiation produces charge carriers in the form of electron-hole pairs. Electrons flow through one electrode connected to the cell, while holes exit through another electrode connected to the cell. The effect is a flow of an electric current through the cell driven by incident solar radiation. Inefficiencies exist in current solar cells due to the inability to collect/use and convert the entire incident light.

[0035] Also, in accordance with a junction design of a PV cell, charge separation of electron-hole pairs is typically confined to a depletion region, which can be limited to a thickness of about 1 μm. Electron-hole pairs that are produced further than a diffusion or drift length from the depletion region typically do not charge separate and, thus, typically do not contribute to the conversion into electrical energy. The depletion region is typically positioned within the PV cell at a particular depth below a surface of the PV cell. The variation of the absorption coefficient of silicon across an incident solar spectrum can impose a compromise with respect to the depth and other characteristics of the depletion region that reduces the efficiency of the PV cell. For example, while a particular depth of the depletion region can be desirable for solar radiation at one wavelength, the same depth can be undesirable for solar radiation at a longer wavelength. In particular, since the longer wavelength solar radiation can penetrate below the surface to a greater degree, electron-hole pairs that are produced can be too far from the depletion region to contribute to an electric current.

[0036] A photoelectrochemical (PEC) cell is a PV cell immersed in an electrolyte to impart electrochemical reactions at its surfaces. It is generally equivalent to electrically connecting a PV cell to two electrodes immersed in an electrolyte such that the electrochemical reactions are directly driven by the electricity generated by the PV. A photoelectrosynthetic (PES) cell is one where the net reactions being driven by the PV cell are thermodynamically unfavorable and thus require the free energy of the PV to perform the reactions. There are two electrochemical reactions, termed half-reactions, that occur, one at each electrode, to result in an overall balanced chemical reaction, such as the water splitting reaction which is $2H_2O \rightarrow 2H_2 + O_2$.

[0037] N/P junction (or p-n or n-p) refers to a connection between a p-type semiconductor and an n-type semiconductor which produces a diode. Depletion region refers to the transition region between an n-type region and a p-type region of an N/P junction where a large electric field exists.

[0038] Electromagnetic Radiation to Electric Energy Conversion Device (EREECD) is a device that reacts with electromagnetic (optical) radiation to produce electrical energy. Optoelectronic Energy Device (OED) refers to a device that reacts with optical radiation to produce electrical energy with an electronic device. As used herein, the term "ultraviolet range" refers to a range of wavelengths from about 5 nm to about 400 nm. As used herein, the term "visible range" refers to a range of wavelengths from about 400 nm to about 700 nm. As used herein, the term "infrared range" refers to a range of wavelengths from about 700 nm to about 2 mm. The infrared range includes the "near infrared range," which refers to a range of wavelengths from about 700 nm to about 5 μm, the "middle infrared range," which refers to a range of wavelengths from about 5 μm to about 30 μm, and the "far infrared range," which refers to a range of wavelengths from about 30 μm to about 2 mm.

[0039] Within this description, the term "semiconductive material", "semiconductor" or "semiconducting substrate" and the like is generally used to refer to elements, structures, or devices, *etc.* comprising materials that have semiconductive properties, unless otherwise indicated. Such materials include, but are not limited to: materials including elements from Group IV of the periodic table; materials including elements from Group III and Group V of the periodic table; materials including elements from Group II and Group VI of the periodic table; materials including elements from Group I and Group VII of the periodic table; materials including elements from Group IV and Group VI of the periodic table; materials including elements from Group V and Group VI of the periodic table; and materials including elements from Group II and Group V of the periodic table. Other materials with semiconductive properties may include: layered semiconductors; metallic alloys; miscellaneous oxides; some organic materials, and some magnetic materials. The term "semiconducting structure" refers to a structure comprising, at least in part, a semiconducting material. A semiconducting structure may comprise either doped or undoped material. As described herein, the "core" or first semiconductive

material can be any semiconductive material. In certain embodiments, the "core" is a Si material.

[0040] Further the term "vertical" with reference to elongated structures, wires, rods, whiskers, pillars, *etc.*, generally refers to structures that have a length direction that is elevated somewhat from horizontal.

[0041] The term "vertical alignment" generally refers to an alignment or orientation of a structure or structures that is elevated from horizontal. The structure or structures do not have to be completely normal to horizontal to be considered to have a vertical alignment.

[0042] The terms "vertically aligned array" or "vertically oriented array" generally refer to arrays of structures where the structures have orientations elevated from a horizontal orientation up to orientations completely normal to a horizontal orientation, but the structures within the array may or may not have all the same orientations with respect to horizontal.

[0043] The term "wider band-gap" refers to the difference in band-gaps between a first sub-cell (or first material) and a second sub-cell (or second material). "Band-gap" or "energy band gap" refers to the characteristic energy profile of a semiconductor that determines its electrical performance, current and voltage output, which is the difference in energy between the valence band maximum and the conduction band minimum. For example, in one embodiment, reference to an elongated structure coated with a material having a "wider band-gap material" refers to a material having a wider band-gap than the elongated structure's material. To drive the water splitting reaction at reasonable overpotentials, ideally the core semiconductive material has a bandgap energy of about 1.1 eV and the outer/radial semiconductive material has an eV of about 1.7 eV.

[0044] Within this description, the terms "wires," "rods," "whiskers," and "pillars" and other similar terms may be used synonymously, except as otherwise indicated. Generally, these terms refer to elongate structures which have lengths and widths, where the length is defined by the longest axis of the structure and the width is defined by the axis generally normal to the longest axis of

the structure. In various embodiments, the diameter of, for example, a "rod" is about 10-50 nm, about 50-100 nm, about 100-500 nm, about 500nm-1μm, about 1μm-10μm or about 10μ-100μm. Typically the diameter will be about 1-10μm. The length of the, for example, "rod" is about 1μm-10μm, about 10μ-100μm, or about 100μm-several millimetres.

[0045] Integrated solar fuels generation devices are of interest to provide chemical energy sources rather than purely electrical energy. In other words, solar cells convert light energy to electrical energy that can be stored or used directly. However, other means to store light energy look to convert the light energy into chemical energy through splitting various chemical to produce H_2. Optimization of various aspects of the components including the semiconductive material, geometry, membranes and flow systems are needed. Tandem semiconductive materials are particularly of interest due to the ability to optimize incident light capture.

[0046] Multi-junction solar cells or tandem cells are solar cells containing several p-n junctions. Each junction can be tuned to a different wavelength of light, reducing one of the largest inherent sources of losses, and thereby increasing efficiency. Traditional single-junction cells have a maximum theoretical efficiency of about 34%, a theoretical "infinite-junction" cell would improve this to 87% under highly concentrated sunlight.

[0047] In addition to band gap considerations for a Si/partner tandem system, achieving the desired electronic behavior at the interface between, *e.g.*, Si and its tandem partner presents a significant challenge for production of an integrated solar fuels generation device. For example, the materials must be mutually compatible and generally must operate in a batch reactor that contains an aqueous electrolyte. Such materials considerations are important to the performance of a functioning device that consists of elongated structures embedded in a gas impermeable, ion-exchange membrane, because both semiconductors are simultaneously in contact with the electrolyte to produce a solar-driven water-splitting device. Tandem junction water-splitting devices using nanoscopic or microscopic materials have focused on a single-junction n–n hetero-

junction design in series with a liquid second junction. In contrast, the highest efficiency water-splitting devices consist of planar tandem homo-junction photovoltaic cells that are physically isolated from the solution and are electrically connected to the catalysts in contact with solution. The materials currently used in high-efficiency planar tandem devices are not sufficiently stable in concentrated aqueous electrolyte environments. Nevertheless, the concept of buried p-n homo-junctions is a promising route to increase the efficiency of solar water splitting devices relative to systems that utilize n-n hetero-junctions.

[0048] To realize the advantages of replacing the n-n hetero-junction with a p-n homo-junction, ohmic behavior at the tandem partner (*e.g.*, Si/partner) interface is used. This ohmic behavior can be achieved in at least two ways: (i) the tandem partners (*e.g.*, the Si-partner) should have proper band alignment (*e.g.*, type III, broken gap) such that upon direct contact, ohmic behavior is produced, or (ii) a discrete intermediate third material must be introduced that facilitates ohmic behavior between the partner light absorbers (*e.g.*, the Si and the tandem partner).

[0049] Embodiments of the disclosure comprise elongated structures comprising a plurality of p-n junctions. In one embodiment, an elongated structure of the disclosure comprises at least two p-n junctions. In another embodiment, the elongated structure comprises 3 or more p-n junctions. A multijunction (sometimes referred to as a tandem junction) device consisting of at least one semiconductive (*e.g.*, Si) elongated structure array and another photopotential generating junction connected in series will improve efficiency and the maximum photopotential, *i.e.* V_{oc}, will also greatly increase. This is important for photoelectrosynthetic systems, where the energy in sunlight is directly converted into chemical fuel. For example, in some instances potentials larger than the V_{oc} of a single Si elongated structure array are required, *e.g.* H_2/Br_3^- from HBr; H_2/Cl_2 from HCl; H_2/O_2 from H_2O, and other reactions where the reduced species contains hydrocarbon and the precursor is CO_2 or carbonic acid or its salts or N_2 or nitrates/nitrities are reduced to amines.

[0050] In one embodiment, the disclosure provides a Si microwire array with a thin emitter layer deposited on the Si microwire. For example, n-type Si elongated structure arrays will be fabricated (n-Si) as described more thoroughly below. Then, a buried-junction will be fabricated as a thin p^+ emitter layer (n-p^+-Si), using, for example, a boron-nitride/-oxide thermal diffusion source wafer or spin-on dopants glass. A layer of transparent conductive material can then be layered onto the surface of the p-n-Si and further followed by application of a radially-integrated hetero semiconductive material having a different band gap than the underlying core n-Si material. For example, low-temperature plasma-enhanced CVD (PECVD), hot-wire CVD (HWCVD), and/or magnetron sputtering can be employed to deposit a thing *a*-p^+-Si layer 9<100 nm). This would result in two p-n junctions connected both optically and electrically in series.

[0051] The disclosure provides a tandem core-shell photoelectrochemical device that comprises a periodic array of buried homo-junction n-p^+ (*e.g.*, n-p^+-Si) elongated structures that have been sequentially coated with a ohmic radial sheath, which is further coated with a second semiconductive material having a different band-gap than the inner (*i.e.*, first or core) semiconductive material (*e.g.*, an n-p^+-Si) elongated structure. As an exemplary embodiment, a tandem core-shell photoelectrochemical device that comprises a periodic array of buried homo-junction n-p^+-Si elongated structure that have been sequentially coated with a radial sheath of transparent conductive material (*e.g.*, a transparent conductive oxide such as ITO) and WO_3 are described herein. When immersed in air-saturated 1.0M H_2SO_4, the dual radial-junction elongated structure enables efficient carrier collection from both the Si and WO_3 light absorbers, despite short minority-carrier diffusion lengths, *i.e.*, ~10 μm in Si and ~1 μm, in WO_3. A feature of this tandem architecture is the incorporation of the ohmic layer (*e.g.*, ITO layer) between the Si and the second semi-conductive (*e.g.*, WO_3) light-absorbing materials. This ohmic contact layer provides facile, low-resistance carrier transport between the Si and second semiconductive material and relaxes the

requirements for a defined band alignment between the p^+-Si emitter and the semiconductive material. As used herein "ohmic layer" or grammatically equivalents thereof, refers to a layer having low resistance. In other words, the ohmic layer does not have to exhibit an ohmic (*i.e.*, linear) I-V response but rather simply be low resistance. For example, a tunnel junction can be considered an ohmic layer (*i.e.*, highly conductive, but does not necessarily exhibit ohmic I-V responses).

[0052] Furthermore, transparent conductive materials are known, and includes for example, transparent conductive oxides (TCOs). Such TCO's are commonly used as back contacts to metal oxides; thus the design of the disclosure provides for a robust implementation because the TCO layer will be amenable to many different Si tandem partner absorbers. Other transparent conductive materials can include nitrides, carbides, chalcogenides and the like.

[0053] Figure 1 depicts an example unit cell of the photoelectrochemical (PEC) device of the disclosure, with one embodiment having rotational symmetry around the vertical axis in the plane of the page. Each elongated structure (**20**) comprises two semiconductors (**20**) and (**30**) with complimentary band gaps, meaning that the sunlight generated photocurrent from each semiconductor is roughly equal when operating at the point of maximum power generation. The semiconductors are arranged electrically and optically in series through a contacting conductor (**40**). In one embodiment, the conductor is transparent. In this embodiment, the transparency affords maximum absorption of sunlight by the underlying core semiconductor (**20**). Absorption of photons generates energetic electron-hole pairs that affect fuel forming chemical reactions at semiconductor-anchored catalysts in intimate contact with the electrolyte solution. One embodiment entails a macroscopic device formed as a two-dimensional periodic array of these dual junction microwires. The periodic array geometry provides increased light absorption over conventional planar devices, per mass of material. This increased absorption results from wave-guiding and light-trapping effects afforded by the array geometry and physical dimensions of the microwires.

[0054] Referring to Figure 1A a schematic of a device (**10**) of the disclosure is depicted. Figure 1A shows an arrangement of a first semiconductive material (*e.g.*, n^+-Si) (**70**) elongated structure with a thin oppositely doped homo-semiconductive material (**60**) (*e.g.*, p^+-Si) deposited on its surface; a transparent conductive material (**40**) is depicted as being coated on the oppositely doped semiconductive material (**60**). The transparent conductive material can be, for example, any transparent conductive oxide (TCO) that provides a low resistance radial sheath. Non-limiting examples of transparent conductive oxides include cadmium tin oxide (CTO), indium tin oxide (ITO), fluorine-doped tin oxide (SnO:F or FTO), indium-doped cadmium-oxide, cadmium stannate (Cd_2SnO_4 or CTO), doped zinc oxide (ZnO), such as aluminum-doped zinc-oxide (ZnO:Al or AZO), indium-zinc oxide (IZO), and zinc tin oxide ($ZnSnO_x$), or combinations thereof. Other conductors include, for example, AZO, GZO, ITO:ZnO, ITO:Ti, In_2O_3, In_2O_3:M (M = Ti, Mo, Ga, W, Zr, Nb), BZO, Al_2O_3, MnO, MgO, and Graphene. The TCO is then coated with a second semiconductive material (**30**) having a wider band gap than the underlying first semiconductive material (**70**). For example, in Figures 1D-F, the wider band gap material is n-doped-WO_3.

[0055] Figure 1D shows an individual two-dimensional unit cell. The highly doped p^+-Si sheath surrounds a moderately doped n-Si elongated structure core, creating a radial n-p^+-Si buried junction. A conformal layer of a TCO (*e.g.*, ITO) surrounds the p^+-Si, forming a transparent ohmic contact between the p^+-Si and the conformal outer semiconductive layer of n-WO_3. A liquid junction is formed between the WO_3 and the solution redox couple (shown as the potential of the oxygen evolution reaction (OER)). In this device, the light absorption and carrier-collection advantage of the n-p^+-Si elongated structure is also extended to the WO_3 photoanode because of its radial-junction geometry with the conformal liquid contact.

[0056] Figure 1D and Figure 1F depict the device electronic band structures in the absence and presence of illumination, respectively. Illumination (Figure 1F) results in splitting of the quasi-Fermi levels at both junctions, generating two voltage sources in series. Photoexcited majority-carrier electrons in the n-Si core

are transported axially to the back contact through the degenerately doped substrate (n^+-Si) to perform the hydrogen-evolution reaction (HER) at a Pt counter electrode, or on the backsides of peeled, freestanding elongated structural arrays, while photoexcited minority-carrier holes are collected radially in the p^+-Si sheath. The holes in Si recombine with photoexcited majority-carrier electrons from the n-WO_3 at the ITO contact, while minority-carrier holes that are photoexcited in the n-WO_3 are collected at the liquid interface and drive the oxidation of water or analyte.

[0057] Absorption lengths for indirect band gap semiconductors like Si are large (*e.g.*, hundreds of microns). In planar Si devices light absorption and minority carrier collection occur on the same coordinate, which requires the collection length to match or exceed the absorption length and thus necessitates high purity material. The Si elongated structure geometry provides a carrier-collection advantage through orthogonalization of the light absorption (long axial dimension) and minority-carrier collection (short radial dimension) axes. These advantages allow less semiconductor material per unit area and lower purity semiconductor material than planar devices. Structuring advantages can also be realized by various other geometries. For example, as shown in Figure 9, pointed or tapered structures or flat tops, can benefit light collection and transduction. Alternative geometries include, but are not limited to, cones, rectangles, pyramids, inverse opals, spheres, ellipsoids, branched wires (like a tree), horn, and dual radii wires to describe a few.

[0058] In Figure 1B, the Si elongated structure of the core is moderately doped n-type ($N_d = 10^{16} - 10^{18}$ cm^{-3}) with a thin, degenerately doped p-type emitter ($N_a > 10^{18}$ cm^{-3}) radial sheath, forming an n-type|p-type (p-n) junction. These doping densities set a lower bound on the wire radius as device performance suffers when the depletion width is greater than the radius of the n-type region. Given the n-type doping densities above and demonstrated degenerate emitters on, *e.g.*, Si elongated structures as small as 100 nm, the lower limit for the radius of the elongated structures can be 136 – 436 nm for $Nd = 10^{18} - 10^{16}$ cm^{-3}, respectively.

[0059] The degenerate p-type sheath is connected electrically to the second semiconductor, which is n-type (Figure 1, photoanode), using a conformal conductor (**40**). For a high efficiency device, this contact must be ohmic to both the photocathode and photoanode. This uniquely identifies this design scheme from alternative ones where more resistive direct semiconductor-semiconductor contacts are present that often result in sub-maximal photovoltages. The photoanode conformally coats the transparent conductor and is in direct contact with the electrolyte, forming either a semiconductor-liquid junction or a buried p^+n-junction near the solution interface. Catalysts are connected electrically to each semiconductor to improve the rates of the chemical reactions and device efficiency. To obtain the largest efficiency, the first semiconductor exposed to sunlight (Figure 1, photoanode) possesses a larger band gap than the inner semiconductor. This arrangement allows below-band gap light to be transmitted through the outer semiconductor to the smaller-band gap semiconductor where it can be absorbed (*e.g.*, Si, whose bandgap is 1.1 eV). Because the semiconductors are also optically in series, this enables current matching between the semiconductors. Extensive material choices exist for both the anode and cathode. For example, such materials include, but are not limited to, Alternative materials include, but are not limited to a-Si, Ge, GaAs, GaP, $CuInGaSe_2$, CdZnSnSe, WSe_2, MoS_2, WS_2, ZrS_2, FeS_2 SiP, SiP_2, Cd_7P_{10}, GeS, Sb_2S, $CuGaSe_2$, Ag, $GeSe_2$, $AgInS_2$, $ZnSiP_2$, $ZnSiAs_2$, $ZnGeP_2$, $ZnGeAs_2$, $CuGeP_2InP$, CdTe, CdSe, CdS, TiO_2, WO_3, SnO_2, ZnO, CuO, CuO_2, $BiVO_4$, Fe_2O_3, $(GaN)_x(ZnO)_{1-x}$, ZnS, InGaN, GaNAs, GaInNAs, GaNP, AlGaAs, AlGaNAs, $ZnSnN_2$, $ZnSnP_2$, Cu_2ZnSnS_4, ZnOSe, ZnP_2, Zn_2P_3, $SrTiO_3$, $BaTiO_3$, In_2O_3, $InVO_4$, $InNbO_4$, $InTaO_4$, TaON, TiON, $PbMo_{1-x}Cr_xO_4$, doped TiO_2 (dopant = N,C, (Cr, C), (Mo, C), (W, C), (V, N), (Nb, N), (Ta, N), (Zr, S), (Hf, S), (2Nb, C), (2Ta, C), (Mo, 2N), (W, 2N), (Ta, P), (Nb, P), (Zr, Se), (Hf, Se)), P3HT:PCBM, PTB4:PCBM, and PTB1:PCBM.

[0060] An ionomer membrane is deposited conformally around the cathode circumference forming an extended, continuous network between all wires in the array (see, Figure 1B and Figure 7). This membrane separates chemical products produced on each side of the

membrane while providing ionic transport through the membrane. Many materials meet these requirements for a membrane. For example, such membrane materials include, but are not limited to, Nafion®, Graphene, Nafion®/SiO_2, Nafion®/ZrP, Nafion®/Pd, Nafion®/polyvinyl alcohol, Nafion®/montmorillonite, Nafion®/Nafion®-PVDF/Nafion®, Sulfonated Polyphosphazene-PBI, Pd, PEO/KOH, Poly(Ech-co-EO), PVA/KOH, PVA/PEch/KOH, PVA/TEAC/KOH, PVA/PAA, PVA/PEO/KOH, Chitosan, PBI/KOH, PEO-$[Si(OCH_3)_3]_2(+)$, PVA-$[Si(OCH_3)_3]_2(+)$, GMA/γ-MPS, Alkoxysilane/acrylate or epoxy alkoxysilane, Poly(VBC-co- γ-MPS), PPO-$Si(OCH_3)_3(+)$, PMA-SiO_2, PVA/TiO_2/KOH, PVA/TiO_2, PVA/ZrO_2/KOH, PVA/PEI cross-linked DBE, PVA/poly(1,3-diethyl-1-vinylimidazolium bromide), PVA/PAAm, PVA/poly(acrylonitrile-co-2-dimethylaminoethylmethacrylate), Quaternized Ech/PAN/DABCO, Poly(ethylene)/poly(St-co-DVB), LDPE/PVB, PP/PVB, PE/PVB, PVDF/PVB, ETFE/PVB, PETE-FEP/PVB, ETFE-FEP/PVB, PS/DVB, LDPF(IPN), LDPE/HDPE(IPN), PS-b-EB-b-PS, PS/butadiene, YSZ, Bi_2O_3, Bi_2O_3-Y_2O_3, ZrO_2-Y_2O_3, ScSZ, CYO, CGO, CSO, (La,Sr)(Ga,Mg)O_{3-x}, $Ba_2In_2O_5$, $La_2Mo_2O_9$, $M_{10}(XO_4)6O_{2+y}$ (M = rare earth or alkaline earth metal, X=P, Si or Ge). In one embodiment, in a water-splitting cell operating under acidic aqueous conditions, the membrane can be a proton exchange membrane such as Nafion®. Mechanical support provided by the membrane enables physical device removal from the growth substrate resulting in a free-standing, flexible PEC device. Device operation follows solid-state drift and diffusion of electrons and holes where two junctions, generally p-n and semiconductor–liquid, drive charge separation under illumination. The resulting photopotential is used to affect chemical reactions such as hydrogen evolution via water splitting. Under solar illumination, photogenerated electron–hole pairs are created in both the elongated structure cores and photoanode shells. Photogenerated carriers in the elongated structure core are separated by the electric field in the radial p-n homojunction. The photogenerated holes are collected radially at the ohmic contact where they recombine with photogenerated majority-carrier electrons from the photoanode. The photogenerated electrons in the core material diffuse axially to the wire base where they are collected at the reductive catalyst to perform the fuel-forming half

reaction. Photogenerated carriers in the photoanode are separated by the electric field in the radial semiconductor–liquid junction. The photogenerated electrons recombine with photogenerated holes from the core material at the transparent conductor, as stated above. The photogenerated holes in the photoanode are collected at the oxidative catalyst where they perform the other fuel-forming half reaction. Many fuel forming reactions can be performed with this design where the initial electron arises from any of a variety of different reactant sources. Exemplary fuels that may be generated include, but are not limited to, H_2, CH_3OH, CH_2O, CH_4, CH_2O_2, CO, C_2H_4, C_2H_5OH, higher hydrocarbons, and reduced N_2. Reactant electron sources include, but are not limited to, H_2O, H_2S, H_2Se, H_2Te, HI, HBr, HCl, HF, NH_3, waste water, and pollutants. The thermodynamic potential required for the desired fuel-forming reaction sets a lower bound to the sum of the semiconductor bandgaps.

[0061] Accordingly, the disclosure provides a tandem multi-junction (*e.g.*, at least two materials) sunlight-to-fuel high aspect ratio array device with appropriate radial dimensions based on doping density, wherein a conformal wider bandgap semiconductor coats the structured cathode, either partially or fully, with appropriate thickness based on minority carrier diffusion length and absorption coefficients, and an intervening conductive material (transparent or non-transparent) that affords an ohmic contact between the photoanode and the core semiconductor. In some embodiment, the device can further comprise a continuous ionomer membrane that keeps reactions products separated and provides mechanical support to the structured device.

[0062] In one embodiment, the wider band-gap material comprises a III-V material. In another embodiment, the wider band-gap material comprises a II-VI material. In yet a further embodiment, the III-V material is selected from the group comprising AlP, GaP, InP, GaInP, AlGaP, AINP, GaNP, InNP, AlGaInP, AIPN, GaPN, InPN, AlGaNP, GaInNP, AlInNP and AlGaInNP. For example, the outer (second) semiconductive material can comprise a semiconductive material selected from the group consisting of GaAs, GaP, $GaAs_xP_{1-x}$, Al_xGa_{1-x}, As, $Al_xGa_{1-x}As_yP_{1-y}$, $In_xGa_{1-x}As$, $In_xGa_{1-x}P$, $In_xGa_{1-x}As_yP_{1-y}$, $Al_xIn_{1-x}As_yP_{1-y}$, $Al_xGa_{1-x}As_yN_zP_{1-y-z}$,

$In_xGa_{1-x}As_yN_zP_{1-y-z}$, Zn_3P_2, Zn_3S_2, and ZnP_xS_{1-x} ($0 \le x \le 1$, $0 \le y \le 1$, $0 \le z \le 1$, $0 \le y+z \le 1$) and any of the semiconductive materials set forth elsewhere herein. In a specific embodiment, the wider band-gap coating material comprises GaP or WO_3. In one embodiment, the wider band-gap coating material comprises a II-VI material. In a further embodiment, the II-VI material is selected from the group consisting of ZnO, CdSe, CdS, CdTe, ZnO, ZnSe, ZnS, ZnTe, CdZnTe, HgCdTe, HgZnTe, and HgZnSe. In yet another embodiment, the wider band-gap material is coated to about 100 nm to about 20 micrometers thick. Furthermore, it should be recognized that any p-type doped regions of the semiconductive material for any portion of the device schematically presented in Figure 1 could be changed to n-type and vice versa.

[0063] Described somewhat differently, Figure 1A depicts a schematic of a radial, integrated tandem elongated structure of the disclosure. The tandem elongated structure (**10**), comprises a first/inner (or core) semiconductive material (**20**) comprising, for example, a first semiconductive elongated structure having an aspect ratio of greater than 1 (**70**). The length of the nanostructure may be 1 micrometer or more (*e.g.*, 1 to 999 micrometers) or may be less than a micrometer in length (*e.g.*, 10 to about 999 nm). In one embodiment, the first semiconductive elongated structure can comprise Si. The elongated structure can be grown from a substrate (as described more thoroughly below), which may be removed, depending upon the ultimate use of an array of such radial-integrated tandem elongated structures. An oppositely doped but similar semiconductive layer (**60**) can be applied to the first elongated structure to encapsulate the first semiconductive elongated structure. An ohmic contact layer (*i.e.*, low resistance layer) (**40**) is then applied first. The ohmic contact (**40**) comprises a transparent conductive material (*e.g.*, TCO). An outer/second (or radial) semiconductive material (**30**) overlays the low resistance material (**40**). The outer/second junction (**30**) can be made of the same or different semiconductive material compared to the first/inner junction (**20**), but will typically be a material having a wider band gap than the inner/first material. In one embodiment,

the "core" or inner semiconductive material is Si and the outer or "radial" semiconductive material is CdSe, WO_3, $BiVO_4$, Fe_2O_2 or amorphous silicon.

[0064] In one embodiment the device comprises an Si elongated structure with dimensions of about 10-80 μm length and about 0.5-2 μm diameter grown by the chemical-vapor deposition, vapor-liquid-solid (CVD-VLS) process. The n-type core is doped with phosphorus (P) to a density of about 5×10^{16} cm^{-3} while the p^+-type shell is doped with boron (B) to a density of about 10^{19} cm^{-3}. The ohmic contact material in this embodiment can be any ohmic material, but in a specific embodiment is indium-tin oxide (ITO) deposited by sputter deposition. The photoanode is titanium dioxide (TiO_2) deposited by electrodeposition, hydrothermal, sputter-deposition or atomic-layer-deposition techniques. Such a system can be used, for example, in a two-electrode electrochemical set-up in acidic H_2SO_4 electrolyte with a platinum counter electrode to affect the HER and TiO_2 on the surface of the Si structure to affect the OER. Each electrode will be in its own compartment of an electrochemical cell separated by a Nafion® proton-exchange membrane. The compartment containing the platinum electrode will be purged to 1 atm of H_2 while the compartment containing the Si-TiO_2 photoelectrode will be purged to 1 atm of O_2.

[0065] The device operates as a solid-state photovoltaic whereby a solid-state Schottky junction is fabricated at the photoanode surface, in place of the electrolyte, and a solid-state ohmic contact is made to the backside of the core microwire array. The height of the photoanode coating can be modulated to increase device efficiency based on material characteristics: absorption (*i.e.*, direct vs. indirect bandgap); contact position (*e.g.*, top of wire only, sides only, everywhere); deposition technique (*e.g.* electrodeposition, sputtering). In another embodiment, the photoanode can also serve as a OER catalyst, removing the need for deposition of an OER catalyst on its surface. In another embodiment, a p-n junction is made in the photoanode by controllably doping with both n-type and p-type dopants. This lessens the design requirements and relative energetics of the semiconductor and OER

catalysts. This device could serve as a fuel forming photo-electro-synthetic device or solid-state photovoltaic device.

[0066] In another embodiment, the catalysis reactions at each material can be swapped, such that photogenerated holes perform the OER at the elongated structure backside (now the photoanode) and photogenerated electrons perform the HER at the outer shell semiconductor, which is now the photocathode. Such an arrangement resembles Figure 1B except that all dopants are opposite of that depicted and the locations of the catalysts are switched. Notably, the photocathode semiconductor coating is p-type.

[0067] In another embodiment an elongated structural core that is moderately doped p-type with a shell that is heavily doped n-type is provided (see, Figure 11). In this embodiment, the heavily doped shell is in contact with the electrolyte and forms an ohmic contact with the HER catalyst. The p-type core is electrically connected to the photoanode through either a transparent conductor (TC) or metallic contact. Transparency is not a required characteristic of this material, because much of the Si microwire is exposed and/or the photoanode-coated region contains highly doped, optically inactive Si. A product-impermeable membrane is deposited between the OER and HER catalysts to separate chemical reaction products, thus increasing overall efficiency.

[0068] In another embodiment, the transparent conductor is replaced with a thin inorganic material or chemically attached monolayer to the Si that allows electronic transport between materials while maintaining material segregation. An ohmic electrical contact is still present in this embodiment.

[0069] In another embodiment, the membrane conformally coats each structured microwire as a thin layer providing vertical ion transport but not mechanical support for the entire microwire array device. Then, a mechanically strong material is placed in between each membrane-coated micro-structure.

[0070] As depicted in Figures 1 and 11, the oxidative catalysts can be placed uniformly, but discontinuously on the photoanode surface. This configuration can lead to deleterious light absorption by the catalyst. Thus, in another embodiment, the deposition and

placement of the oxidative catalyst as a discontinuous network in direct physical contact with the top of the membrane and in electrical contact with the photoanode can afford increased light absorption in the semiconductors.

[0071] In yet another embodiment, scattering dielectric particles are suspended in the membrane or in a discontinuous network above the membrane, and/or above the catalysts, described above, to increase light absorption in the semiconductors and hide the strongly absorbing catalysts from light (if they are placed in a network below the scatterers).

[0072] In one embodiment, the core semiconductor has a p–i–n doping configuration and operates under high-level injection, but still generates a V_{oc} that is similar to that obtained for a typical p-n junction. For example, the device in Figure 1 could comprise an n-type base with an intrinsic core and a p-type sheath. The n- and p-type regions could be doped higher than in Figure 1, if their respective volumes are kept small.

[0073] The disclosure also provides a method of making a radially-integrated tandem elongated structure array of the disclosure. Figure 2A shows a photolithographically patterned n^+-Si<111> wafer (**35** (**20** in Figure 1A)) with a SiO_2 mask layer (**25**) and Cu catalyst (**15**) in the desired growth patterned holes. Other materials may also be used to support growth of an elongated structure, such as a thin Si layer disposed on glass, or other such Si substrates. All or portions of the wafer may be doped. For example, some embodiments may use a degenerately doped n-type Si wafer. In the process a surface oxide layer is thermally grown on the wafer. In one embodiment, the surface oxide layer is grown to a thickness of 285 nm. In another embodiment, the surface oxide layer is grown to a thickness of 300 nm. Other embodiments may comprise oxide layers at other thicknesses. Still other embodiments have the oxide layer deposited via chemical vapor deposition (CVD) or other methods known in the art. Use of the oxide layer is particularly useful in some embodiments of the disclosure. For example, Si wire arrays did not yield high pattern fidelity when the catalyst was not confined using the patterned oxide layer as described above.

[0074] The photoresist layer is applied to support the development of a patterned template as discussed below. However, other materials and techniques for creating a patterned template may be used, such as a latex layer, or stamping or soft lithography. The photoresist layer may comprise S1813 photoresist from MicroChem Corp. (Newton, Mass., USA) or other photoresist material. The photoresist layer is then exposed to ultraviolet-to-visible light through a desired array pattern and developed with a developer to form a desired pattern of holes in the resist layer. The developer may comprise MF-319 or other developers known in the art. The patterned resist layer is then used to etch the oxide layer on the Si wafer. Etching of the oxide layer may be achieved by using hydrofluoric acid compositions such as buffered HF (9% HF, 32% NH_4F) from Transene Company, Inc. (Danvers, Mass., USA). Other etching techniques known in the art may also be used to etch the oxide layer. The result of the etching will be a pattern of holes in the oxide layer. A pattern of holes may be, for example, a square array of 3 μm diameter holes that are 7 μm center to center.

[0075] The growth catalyst (**15**) is then thermally evaporated onto the resist layer and into the holes in the oxide layer. Other methods of depositing the catalyst may be used, such as electrodeposition. Typical catalysts comprise gold, copper, or nickel, but other metals known in the art as Si V-L-S catalysts may be used, such as platinum or aluminum. For example, 500 nm of gold may be thermally evaporated onto the resist layer and into the holes. Lift-off of the photoresist layer is then performed, leaving catalyst islands separated by the oxide in the oxide layer. Cost also motivates the use of non-Au catalysts for embodiments according to the disclosure. As indicated above, Cu, Ni, Pt, or Al may be used as a catalyst for Si structure growth. Cu is, unlike Au, an inexpensive, earth-abundant material, and, therefore, of particular interest for such embodiments. Although Cu is more soluble in Si than Au and is also a deep trap, Si solar cells are more tolerant of Cu contamination than of Au, and thus diffusion lengths of at least microns even in the case of Cu catalyzed growth can be expected. As discussed above, other growth catalysts may be used to facilitate

the growth of the Si elongated structure in the array. Nominally identical elongated structural arrays may be obtained when Cu, Ni, Pt, or Al (or other Si growth catalyst metals) are used as the VLS growth catalyst instead of Au.

[0076] The wafer with the patterned oxide layer and the deposited catalyst may then be annealed. Typically, the annealing is performed in a tube furnace at a temperature between 900 to 1000 °C or at a temperature of about 1050°C for 20 minutes with the application of 1 atm of H_2 at a flow rate of 1000 sccm (where SCCM denotes cubic centimeters per minute at STP). Growth of elongated structures on the wafer is then performed (Figure 2B). Typically, the elongated structures are grown in a mixture of H_2 (1000 sccm) and $SiCl_4$ (20 sccm) at about 1 atm, along with dopant precursors (*e.g.*, BCl_3 for B (p-type) doping and PH_3 for P (n-type) doping). In one embodiment, the elongated structures are grown for between 20 to 30 minutes at temperatures between 850°C to 1100°C. Other embodiments may use different growth times, pressures, and or flow rates. However, optimal growth temperatures are between 1000°C and 1050°C. Growth for these times and at these temperatures may produce elongated structures from 10 µm to 30 µm in length or longer (Figure 2C). This SiO_2 layer (**25**) can be formed by (i) dry SiO_2 growth, or (ii) infill of polymethyldisiloxane (PMDS) as an etch mask.

[0077] Following the growth of the elongated structures, the oxide layer may be removed; however, it is not necessary for the oxide layer to be removed. Removal of the SiO_2 by HF etching of the exposed SiO_2 portions on the Si elongated structures or PDMS removal can be performed (Figure 2C). Growth catalyst particles may remain at the top of each grown elongated structures, which may impact the functionality of the resulting array. Therefore, it may be advantageous to remove the catalyst particles. For example, if the catalyst comprises Au, the gold particles may be removed by soaking the wafer 10 for 10 min in a TFA solution from Transene Company, Inc., which contains I^-/I_3^-. Other methods known in the art may also be used to remove catalyst particles.

[0078] A highly doped p^+-Si radial sheath (**55** or (**60**; Fig. 1)) is formed by chemical-vapor deposition (CVD) of boron from a BCl_3

precursor at 950 °C for 30 min (Figure 2D). A 400 nm planar equivalent layer of a transparent conductive oxide (**65** or (**40**; Fig. 1)) (*e.g.*, ITO) is then DC-sputtered conformally on the elongated structures, which has been shown to make ohmic electrical contact to p^+-Si (Figure 2E). A film of a second semiconductive material (**75** or (**30**; Fig. 1)) having a different band gap than the underlying Si elongated structure (*e.g.*, n-WO_3) is then electrochemically deposited, and annealed at 400 °C for 2 h, to form the radially-integrated tandem elongated structure (Figure 2F).

[0079] According to an embodiment of the disclosure, photolithography is a suitable method for enabling uniform arrays of elongated structures of diameters of ~1 μm to be grown over large areas. In cost sensitive applications such as photovoltaics, it may be desirable to employ lower-cost lithographic methods, and embodiments of the disclosure are readily extendable to alternative patterning techniques such as nanoimprint lithography.

[0080] The method described above has been shown to produce nearly defect-free arrays that exhibited an extremely narrow diameter and length distribution, and highly controlled elongated structure position.

[0081] In one embodiment, the elongated structures in an array can be embedded in a glass, polymer wax or other material. Of particular interest are proton conducting membranes (*e.g.*, Nafion®). The embedding material can be used to mechanically peel the elongated structure array from the substrate to make a free-standing device. This free-standing device can be contacted electrically to external leads, thus forming a PV cell, or immersed in an electrolyte, after possible deposition of appropriate electrocatalysts, to form a PES cell. Also, ITO could be deposited on the top of this device to make a solid-state PV. In yet another embodiment, a catalyst (*e.g.*, Pt, Ni, Ni-Mo, MoS_2 or the like) can be coated on the device to facilitate H_2 production from H_2O, or other electrochemical half-reactions resulting in a photoelectrosynthetic cell. (See Figure 7).

[0082] The disclosure also demonstrates that geometry of the material can assist in maximizing the efficiency of the

photoelectrochemical device. Elongated structures of the disclosure have multiple advantages over the traditional, single, planar photoelectrode model, including (i) serving as a scaffold for the deposition of an ohmic contact and photoanode material ("monolithic") to allow for the combination of both materials' photovoltages in series to attain sufficient voltage to split water, while simultaneously absorbing visible light, (ii) the orthogonalization of light absorption (axial) and carrier transport(radial), which is especially advantageous for indirect bandgap semiconductors, which have long absorption lengths, (iii) increased surface area for catalysis, (iv) approximately a 90% decrease in photoelectrode material usage compared with the planar alternative, depending on pitch and diameter of the elongated structure, (v) radial strain relief for epitaxial growth, enabling the combination of lattice mismatched materials and (vi) logical incorporation of ion-conducting membrane for gas separation and minimization of the distance and resistance of ion migration between the anode and cathode compartments. Nevertheless, nano- and micro-structured devices often exhibit lower open circuit voltages, V_{OC}, than their planar counterparts because of the increased junction area, which increases the dark current. The V_{OC} can be calculated from the following equation, where n is the diode quality factor, k_B is Boltzmann's constant, q is electric charge, J_L is the photogenerated current, γ is the ratio of the junction area to the planar area, and J_0 is the reverse saturation dark current:

$$V_{oc} = \frac{nk_B T}{q} \ln(\frac{J_L}{\gamma J_0} + 1)$$

[0083] This equation indicates that a 10-fold increase in junction area results in a ~60mV loss in V_{OC}. The decrease in VOC due to increased junction area is an effect of a decreased splitting in the quasi-Fermi levels because the light-generated charge carriers are less concentrated. Despite this disadvantage, micro-structured devices are expected to enhance performance with respect to the planar alternative, provided that (i) the diffusion length, L_D, is shorter than the inverse of the absorption coefficient, α, and (ii) the depletion width carrier lifetimes, $\tau_{p,D}$ and $\tau_{n,D}$, are large.

Because silicon is an indirect gap material, the first parameter of $L_D << \alpha^{-1}$ is inherently satisfied when the Si is an type but the purest form.

[0084] The efficiency of a PEC device, η_c, depends on the power/irradiance of the incident solar flux, P_{in}, the absorbed photon flux, J_a, the internal quantum efficiency of the photoelectrode, φ_{int}, and the reaction potential difference:

$$\eta_c = \frac{J_a \varphi_{ing} \Delta E^0}{P_{In}}$$

[0085] In a tandem cell design, the relevant absorbed photon flux and internal quantum efficiency is that of the current-limiting material. Because efficiency is linearly proportional to the amount of light absorbed, maximizing light absorption is integral to achieving a high efficiency device. The following explores techniques to optimize light absorption in the WO_3 photoanode material in combination with Si as the photocathode.

[0086] Using the modeling described herein, an optimized structure for the transparent contact design is a 5µm pitch array of spearshaped silicon elongated structure, coated conformally with 100nm of a transparent contact material with a refractive index in the range of 1.4 to 1.6, subsequently coated in 1µm of WO_3, which has a flat top coated in 100nm of SiO_2, all on top of a back reflector.

[0087] Embodiments of the disclosure provide structures that are particularly useful for devices such as solar cells, electronic devices, photonic materials that utilize optical properties of periodic structures of light-absorbing or light-directing materials arranged with structural order in another optically different material, sensors, fuel-forming artificial photoelectrosynthetic solar fuels devices, and similar chemical, optical, and electronic devices and structures.

[0088] Embodiments of the disclosure comprise arrays of elongated structures or other semiconducting structures with control of the size, position, and uniformity of the fabricated arrays or structures over a relatively wide area wherein the arrays comprise elongated structures having tandem or multijunction modes. Such

arrays of elongated structures can comprise crystalline Si elongated structures of a length long enough to absorb a significant fraction of above-bandgap sunlight, each elongated structure with a radius matched to its diffusion length, and the elongated structures being regularly spaced, and oriented predominantly vertically, typically over large areas. As mentioned herein, the dimensions of the underlying arrays of elongated structures are typically from about 1-10μm in diameter and 10-100μm or greater in length. Embodiments of the disclosure may comprise growing the arrays or structures through VLS processes.

[0089] Such arrays or structures comprise, in one embodiment, crystalline Si elongated structures of a length long enough to absorb a significant fraction of above-bandgap sunlight, each elongated structure with a radius matched to its diffusion length, and the elongated structures being regularly spaced, and oriented predominantly vertically, typically over large areas. Embodiments of the disclosure can comprise growing the arrays or structures through VLS processes. In such an embodiment, a templating layer is first patterned with openings (*e.g.*, an array of holes) in which the elongated structures are to be grown. The templating layer comprises a diffusion barrier for a deposited catalyst. The diffusion barrier may comprise a patterned oxide layer, a patterned insulating layer, such as a layer comprising silicon nitride, a patterned metal layer, or combinations of these materials or other materials or processes that facilitate the deposition of the catalyst for semiconductor structure growth. The catalyst is then deposited in the openings. Elongated structures are then grown on the substrate by heating the substrate and applying a growth gas.

[0090] The elongated structures are then modified to include a p-emitter layer and a radial ohmic layer. This ohmic layer can be selected based upon the ohmic properties as well as its reflective and transparent properties. The ohmic layer can be subsequently coated with an outer radial and epitaxial second semiconductive material having a different band-gap than the underlying core Si elongated structure. The geometry and thickness of the outer radial

and epitaxial semiconductive material can be designed to optimize collection of incident light.

[0091] The ordered array of elongated structures (*e.g.*, rods/wires) can then be embedded in a matrix material (*e.g.*, glass, wax or a polymer). The array can be embedded to substantially cover the whole length of the elongated structures (*e.g.*, 1-100% of the length), or may be only partially embedded (*e.g.*, 99% or less). The matrix can be useful for removing the array of elongated structures from a substrate. For PES devices the embedding material is typically a proton conducting polymeric material that allows protons to pass from the photoanode side to the photocathode size of the membrane (see Figure 7).

[0092] Thus, in one embodiment the disclosure provides an array of elongated structure (*e.g.*, rods/wires) comprising Si having dimensions of about 1-10 micrometers in diameter and about 1 micrometer to about 100 µm in length coated with one or more layers of the opposite (p/n)-type silicon to form a p-n junction. In some embodiments, the array of elongated structures (*e.g.*, rods/wires) is generated on a substrate. The elongated structures are then coated with a TCO material and a subsequent second radial and epitaxial semicondcutive material having a different band gap than the Si.

[0093] A particular application for arrays of elongated structures fabricated according to embodiments of the disclosure are for the use of such arrays in photoelectrochemical cells (PEC) or photoelectrosynthetic (PES) fuel-generating systems. Device analysis has shown that photovoltaic efficiency is maximized in arrays when the mean radius of the elongated structures is comparable to the minority carrier diffusion length. This is because of a trade-off between increased current collection and the loss of open-circuit voltage due to the increased junction and surface area. Diffusion of gold into bulk silicon at the growth temperatures of 1000-1050 °C leads to carrier lifetimes of >1 ns, which combined with carrier mobilities expected for the observed dopant densities, indicates minority carrier diffusion lengths of ~1 µm. However, as described herein, embodiments of the disclosure provide the ability to grow relatively long wire arrays (greater than 30 µm) while

maintaining a radius comparable to the minority diffusion length (on the order of 1.5 μm). In some embodiments, these arrays are coated with about 100 nm thick layer of an opposite-type Si emitter layer to give a total layered diameter of about 2.5 micrometers.

[0094] Hence, embodiments of the disclosure provide elongated structural arrays with aspect ratios particularly suitable for use in solar cell apparatus. Further, embodiments of the disclosure provide for the ability to have relatively dense arrays of elongated structures, further improving the ability of devices using such arrays to convert light to electrical energy.

[0095] The disclosure also provides an artificial photo(electro)synthetic system that utilizes sunlight and water, or other solutions that can be used to generate H_2, gas as inputs and produces hydrogen and, for example, oxygen as the outputs. The system comprises three distinct primary components: a photoanode, a photocathode, and a product-separating but ion-conducting membrane. These components may be fabricated and optimized separately before assembly into a complete water-splitting system. The system may incorporate two separate, photosensitive semiconductor/liquid junctions that collectively generate, for example, the 1.7-1.9 V at open circuit necessary to support both the net oxidation and reduction of, for example, water to O_2 and H_2, respectively.

[0096] The photoanode and photocathode may comprise arrays of semiconductive elongated structures of the disclosure comprising a metal catalyst on an amorphous-p^+in^+Si cap in tandem with the semiconductive elongated structure, as described herein. The catalysts disposed on the semiconductive structures are used to drive the oxidation or reduction reactions at low overpotentials. Typically the catalysts coated on the semiconducting structures/substrates do not block or inhibit light energy from contacting the semiconducting array or substrate. Accordingly, the catalyst should cover from about 1-99% of the surface area unless sufficiently transparent to allow light penetration to the underlying semiconducting substrate. The high aspect-ratio semiconductor elongated structure electrodes allow for the use of low cost, earth abundant materials without sacrificing energy

conversion efficiency due to the orthogonalization of light absorption and charge-carrier collection. Additionally, the high surface-area design of the elongated structure-based semiconductor array electrode inherently lowers the flux of charge carriers over the rod array surface relative to the projected geometric surface of the photoelectrode, thus lowering the photocurrent density at the solid/liquid junction and thereby relaxing the demands on the activity (and cost) of the electrocatalysts. A flexible composite polymer film may be used to allow for electron and ion conduction between the photoanode and photocathode while simultaneously preventing mixing of the gaseous products. That is, the elongated structure arrays may be embedded in flexible, polymeric membrane materials, allowing the possibility of roll-to-roll system assembly. Separate polymeric materials may be used to make electrical contact between the anode and cathode, and also to provide structural support. Interspersed patches of an ion conducting polymer may be used to maintain charge balance between the two half-cells.

[0097] In a particular embodiment, the photocathode may comprise vertically (or near vertically) aligned elongated structure arrays made of macroporous p-Si <100> with a resistivity of 13-15 Ω cm and coated/capped with an amorphous p^{+}-in^{+}-Si cap in tandem with the array of elongated structures.

[0098] In another embodiment, the photoanode and photocathode components may be electrically, and ionically, interconnected through, but physically separated by, a flexible composite polymer film. Further, multi-component membranes, composed of polymeric materials, that exhibit desired mechanical pliability, electronic conductivity, and ion permeability properties for a feasible water electrolysis system may be used. Specifically, polypyrrole may be used to make electrical contact between the anode and cathode, while poly(dimethylsiloxane) (PDMS) may be used to provide structural support for the elongated structure arrays. For proton conduction in a cell operated under acidic conditions, Nafion® may be employed, whereas vinylbenzyl chloride modified films of poly(ethylene-co-tetrafluoroethylene) (ETFE), or amine-modified sulfonyl fluoride

Nafion® precursors, may be used for hydroxide conduction in a cell operated under alkaline conditions.

[0099] In yet another embodiment, a catalyst such as a hydrogen or oxygen evolution catalyst can be coated on the device to facilitate, for example, H_2 production from H_2O. The catalyst can be any number of catalysts useful as hydrogen or oxygen evolution. For example, suitable hydrogen evolution catalyst can be selected from the group consisting of Pt, Co, Cu, Fe, MoS_x where x is nominally 2, but may be sub or super-stoichiometric, Ni, CoMo, CoW, FeMo, NiCo, NiFe, NiFeC, NiFeS, NiMnS, NiMo, NiMoP, NiSn, NiW, NiZn, NiZnP, CoNiFe, NiCoPMo, NiMoCo, NiMoCu, NiMoFe, NiMoW, NiSiMo, NiSiW and NiWPCu. Suitable oxygen evolution catalysts that can be used in the methods and composition of the disclosure can be selected from the group consisting of IrO_x where x is nominally 2, but may be sub or super-stoichiometric, Pt, Co, $Co/(PO_4)^{3-}$, $Co/(BO_3)^{3-}$, CoP, Cu, Fe, Mn, Ni, $Ni/(BO_3)^{3-}$,NiP, Pb, CoFe, $CoPSc_2O_3$, FeMn, NiCo, NiCr, NiCu, NiFe, NiLa, NiLa, $NiPSc_2O_3$, NiSn, NiZn and NiMoFe. For example, photocathode side of the membrane can be coated with a hydrogen reduction catalyst such as Pt, or other catalysts that are needed to produce the desired fuels. Where Si elongated structures extend out from the membrane on the photocathode side the elongated structure can be coated with a hydrogen evolution catalyst (see, Figure 7). Similarly, the photoanode side of the membrane comprises the tandem-radially integrated elongated structure arrays. On the photoanode side the elongated structures are coated with oxygen evolution catalysts. (see Figure 7).

[00100] The following examples are meant to illustrate, not limit, the disclosed invention.

EXAMPLES

[00101] **Chemicals.** All chemicals were used as received unless noted otherwise. Water was filtered using a MilliPore system and had a resistivity > 18 MΩ-cm.

[00102] **Si Microwire Array Growth.** Phosphorous-doped (N_D =3 x 10^{17} cm^{-3}) and boron-doped (N_A = 1 x 10^{17} cm^{-3}) Si microwire arrays were grown via a Cu-catalyzed vapor-liquid-solid (VLS) process on As-doped n^+-Si or on B-doped p^+-Si <111> wafers (<0.005 Ω-cm, Addison).

The n^+-Si and p^+-Si <111> growth wafers were received with a 400 nm thick thermal oxide (SiO_2) that had been patterned to produce 3 µm diameter holes filled with Cu on a 7 µm pitch The growth of Si microwire arrays was performed in a chemical-vapor deposition (CVD) furnace at atmospheric pressure using $SiCl_4$ (Strem, 99.9999+%) at 25 sccm flow rate, H_2 (Matheson, research grade) at 500 sccm flow rate, and BCl_3 (Matheson, 0.25% in H_2) at 1 sccm flow rate for 20 min or PH_3 (Matheson, 100ppm in H_2) at 0.3 sccm flow rate for 9 min. This process produced Si microwires that were 40-70 µm in length, had a diameter of~ 2 µm and had doping densities on the order of 10^{17} cm^{-3}. Following growth, the samples were cooled to ~ 200 °C under a 500 sccm flow of He.

[00103] Microwire Array Cleaning and Booting. Microwire arrays were cleaned using a 6:1:1 (by volume) H_2O:HCl(fuming, aqueous):H_2O_2(30% in H_2O) metal etch (RCA 2) for 20 min at 60 °C. The samples were then subjected to a 15 s etch in buffered HF(aq) (BHF) etch, an H_2O rinse, an organic (piranha) etch in 3:1 H_2SO_4(99.6%, aqueous):H_2O_2(30% in H_2O) for 10 min at room temperature, and an H_2O rinse. Following a 30 s etch in 10% BHF and a rinse with H_2O, a 150 nm thick SiO_2 layer was grown via dry thermal oxidation in a tube furnace at 1050 °C under an O_2 atmosphere for 2.5 h. A 15 µm thick PDMS layer was deposited at the base of the wires by spin coating a solution, consisting of 1.1 g of polydimethylsiloxane (PDMS, Sylgard 185, Dow Corning) and 0.1 g of PDMS curing agent dissolved in 5 mL of toluene, on the sample at 3000 rpm for 30 s, followed by a 30 min cure in vacuum oven at 150 °C. These PDMS-infilled arrays were submerged in BHF for 5 min, to remove the SiO_2 on the exposed microwire surfaces. The PDMS was removed by a 30 min soak in 3:1 N-methyl-2-pyrrolidone(NMP):tetrabutylammonium fluoride(TBAF), followed by a 30 s rinse with H_2O. The samples were then dried under a stream of N_2(g). Residual organics were then removed by a 10 min etch in a piranha solution.

[00104] p^+-Si Emitter Formation on n-Si. A boron-doped p^+-Si radial emitter was formed on the n-Si microwire arrays and on planar <111> n-Si wafers (Silicon Inc., 0.7Ω-cm) by exposure of the samples in a CVD furnace to a 20:400 sccm flow of BCl_3 (Matheson, 0.25% in

H_2):H_2(Matheson, research grade) at 950 °C for 30 min, immediately following a 30 sec etch in 10% BHF. The samples were then rinsed with H_2O and dried under a stream of N_2(g). Secondary ion mass spectrometry data from the planar samples indicated that the emitter thickness was ~ 200 nm.

[00105] Deposition of ITO. Immediately following a 15 sec etch in 10% BHF, a rinse in H_2O and drying under a stream of N_2(g), 400 nm of In-doped tin oxide was sputtered (48 W, 3 mTorr, 20:0.75 sccm Ar:10% O_2 in Ar) onto n-p^+-Si microwire arrays and p-Si microwire arrays, by DC magnetron sputtering under 10 W of substrate bias (to facilitate conformal deposition on the microwire sidewalls). The thickness of the ITO was determined by spectroscopic ellipsometry measurements on a planar Si sample.

[00106] WO_3 Deposition. n-WO_3 was electrodeposited from a tungstic peroxy-acid solution. Briefly, 4.6 g of tungsten powder (0.6-1μm, 99.99%, Sigma Aldrich) was dissolved in molar excess (60 mL) of H_2O_2 (30% in H_2O). Excess H_2O_2 was dissolved by addition of a trace amount of Pt black (99.9%, Sigma Aldrich) for 24 h. The H_2O_2 concentration was monitored by peroxide test strips (EM Quant) until final peroxide concentration was < 30 ppm. A concentrated stock solution was made by addition of 80 mL of H_2O and 60 mL of isopropyl alcohol (IPA) to the as made solution. To increase its lifetime, the stock solution was protected from light and stored at 2°C in a refrigerator. A 3:7 IPA:H_2O mixture was used to dilute the stock solution (3:2 IPA/H_2O mix:stock solution) to generate the deposition solution. Stock solutions were used for one week before and thereafter were freshly prepared. All ITO-coated samples were used as prepared for deposition of WO_3, and were contacted directly to the ITO layer using a flat alligator clip. Deposition of WO_3 on n-p^+-Si and p-Si microwire arrays was performed potentiostatically at -0.5 V vs Ag/AgCl for 60 min. After deposition, all samples were annealed in air at 400 °C for 2 h. This process formed monoclinic WO_3, as confirmed by X-ray diffraction data. Cross-sectional SEM data indicated that the WO_3 films were ~400 nm thick on Si microwire arrays.

[00107] **Electrode Fabrication.** Three types of electrodes were tested: n-p^+-Si microwire arrays; n-p^+-Si/ITO/WO_3 microwire arrays; and p-Si/ITO/WO_3 microwire arrays. To make ohmic contact to Si substrates that supported the microwire arrays, In-Ga (99.99%, Alfa-Aesar) eutectic was scratched into the back-side of the samples. Exposed In-Ga (Si electrodes) was affixed to a coiled Cu-Sn wire with Ag paint (SPI 05001-AB). The active area (~ 0.12 cm^2 for Si microwire arrays) was defined with epoxy (Loctite Hysol 9460) and the entire electrode was sealed with epoxy to the bottom of a glass tube (6mm O.D.). The electrode orientation, down- or side-facing, was determined by the orientation of the coiled wire that protruded from the glass tube. Geometric areas were measured by scanning the active area, and using software (ImageJ) to calculate the area.

[00108] **Non-Aqueous Photoelectrochemistry.** Bottom-facing electrodes that contained n-p^+-Si microwire arrays were etched for 30 s in 10% BHF immediately prior to introducing the samples into a glove box. Solutions for PEC measurements consisted of CH_3CN (anhydrous, 99.8%, Sigma Aldrich) distilled under N_2(g) (ultra-high purity, Air Liquide) from calcium hydride (CaH_2), 1M $LiClO_4$ (battery grade, 99.99%, Sigma Aldrich), and either 25 mM bis(cyclopentadienyl) iron(II) (ferrocene, $FeCp_2^0$, Sigma Aldrich) and 3 mM bis(cyclopentadienyl) iron(III) tetrafluoroborate (ferrocenium, $FeCp_2^+BF_4^-$, Sigma Aldrich), or 20 mM bis(cyclopentadienyl) cobalt(II) (cobaltocene, $CoCp_2^0$, Sigma Aldrich) and 2 mM bis(cyclopentadienyl) cobalt(III) hexafluorophosphate (cobaltocenium, $CoCp_2^+PF_6^-$, Sigma Aldrich). Cobaltocene and ferrocene were purified by vacuum sublimation at room temperature, and cobaltocenium and ferrocenium were recrystallized prior to use. An ELH-type W–halogen lamp with a dichroic rear reflector was used for illumination, and was set to produce the same current density on a calibrated Si photodiode as was obtained from 100 mW-cm^{-2} of 1 Sun AM1.5 G illumination. Three-electrode PEC data were obtained in a single-compartment cell by use of a Gamry potentiostat (Reference 600), with a Pt counter electrode and a Pt quasi-reference electrode at scan rates of 20 mV-s^{-1}.

[00109] **Aqueous Photoelectrochemistry.** Side-facing planar and microwire array (p-Si/ITO/WO_3, n-p^+-Si/ITO/WO_3) devices were tested in 1 M H_2SO_4(aq) (trace metal grade, Fischer Scientific) saturated with air. Multiple devices were tested (>5) with the reported results representing the best performing devices. Two-electrode and three-electrode measurements were conducted using a Biologic (SP-200) potentiostat in a two-compartment cell (whose compartments are referred to as the anode compartment and the cathode compartment) that contained an epoxied (Loctite Hysol 1C) quartz window on the anode side and a Nafion® (0.05 mm thick, Alfa Aesar) membrane separator between the compartments. Illumination was produced by a Xe lamp (Oriel 67005, Newport Instruments) with an AM1.5G filter (Newport Instruments 81094) that produced light intensities of either 1 (100 mW-cm^{-2}) or 12 (1080 mW-cm^{-2}) Suns on a calibrated Si photodiode. The concentration value (12x) was determined using the AM1.5D spectrum to be consistent with what would be expected in outdoor testing, although an AM1.5G source was used. Calibration was performed such that the highest light intensity anywhere in the cell was at the cited light intensity and the position of the photodiode at this light intensity was marked to assure sample positioning was at the same point. Optical concentration was achieved using a plano-convex lens (Thorlabs LA4984). The spot size (~1cm^2) overfilled all samples tested (~0.1cm^2).

[00110] **Three-Electrode Measurements.** Three-electrode measurements were conducted with the working electrode in the anode compartment open to air, an SCE reference electrode (CH Instruments, CHI150) in the anode compartment, and a Pt mesh counter electrode in the cathode compartment at a scan rate of 20 mV-s^{-1}. Pt disc (0.0314 cm^2) three-electrode measurements were performed with the Pt disc in the cathode compartment and with the SCE reference and the Pt mesh counter electrodes in the anode compartment. For Pt disc measurements, the cathode compartment was saturated with either Ar(g) (research grade, Air Liquide) or H_2(g) (research grade, Air Liquide) by bubbling for 15 min before testing and throughout the experiment. All the measurements were referenced to the potential

of the RHE ($E(H^+/H_2)$), obtained empirically using the Pt disc electrode under 1 atm of H_2(g), -0.247 V vs. SCE.

[00111] **Two-Electrode Measurements.** Two-electrode measurements were made in the same two-compartment cell as used for the three-electrode measurements and with the electrodes in the same physical location. The cathode compartment was purged with Ar(g) or H_2(g). A Pt disc electrode was used as the cathode, to simulate the expected catalyst area for an integrated device. The anode compartment contained the working electrode, which was illuminated through a quartz window and was open to air. Chromoamperometric measurements were taken under potentiostatic control at 0 V applied bias between the photoanode and cathode.

[00112] **Load-line Analysis.** The Pt disc *I-E* data were mirrored about the abscissa, to facilitate straightforward evaluation of the projected electrochemical operating conditions of the device. The Pt disc data include the solution and membrane resistances, because the reference electrode was in the opposite cell as the Pt electrode during the measurement. Hence, the Pt disc data should account for all expected cell resistances in the system of interest. The predicted operating currents from the load-line analysis were calculated based on the average of the forward and reverse scans and are $6.7x10^{-3}$ mA ($6.1x10^{-3}$ mA-cm^{-2}) and $2.6x10^{-3}$ mA ($2.1x10^{-3}$ mA-cm^{-2}) for the Ar(g)- and H_2(g)-saturated solutions, respectively. The current densities are calculated per geometrical surface area of the electrode.

[00113] **Light Absorption Simulation.** Light absorption was simulated in Lumerical FDTD, a commercially available Maxwell's equation solver that uses the FDTD method. The software requires material-specific refractive index data. Experimentally fabricated structures were reproduced in the Lumerical workspace in 2D. Bloch boundary conditions were used to model an infinite planar structure and an infinite 2D microwire array. Each structure was illuminated with single-wavelength plane waves with the electric field polarized in the 2D structured plane, at wavelengths ranging from 350 to 1100 nm in 50 nm intervals. Partial spectral averaging was used to remove simulation artifacts that were caused by the use of single-

wavelength simulations. The structure was meshed with 20 mesh boxes per wavelength. The spatially resolved electric field, E, and complex refractive index (Є) were recorded and then used to calculate the spatially resolved carrier generation rate, C_{gen} (Equation 1):

$$C_{gen} = \frac{\pi |E|^2 imag(\varepsilon)}{h} \qquad (1)$$

where h is Planck's constant. The spatially resolved carrier generation rate was used as the optical input for the electronic simulations. The power absorbed in each material was calculated by integrating the spatially resolved absorbed power, P_{abs} (Equation 2).

$$P_{abs} = -0.5\omega |E|^2 imag(\varepsilon) \qquad (2)$$

The absorbed photon flux in each material as a function of wavelength was weighted with the AM1.5G spectrum, integrated over wavelength, and multiplied by Faraday's constant to obtain a short-circuit current density assuming unity internal quantum yield (IQY). The concentrated illumination modeling was performed at 11 Suns using the AM1.5G spectrum to match the experimental photon flux.

[00114] Electronic Simulations. Electronic simulations were performed in Synopsys Sentaurus, a commercially developed software package that solves the drift-diffusion equation for charge carriers using a finite-element method. For simplicity, a single n-p^+-Si homo-junction and an n-WO_3/$E^{o\prime}$(O_2/H_2O) liquid junction were modeled separately.

[00115] n-p^+-Si junction. The built-in materials parameter file for Si was used with modified time constants (τ_n(N_A=10^{20}cm^{-3}) = 3x10^{-6} s; τ_p(N_D=10^{17}cm^{-3}) = 1x10^{-3} s). The silicon p^+-n junction was constructed with a 100 μm thick n-region with N_D=10^{17}cm^{-3} and a 0.2 um thick p^+-region with N_A=10^{20} cm^{-3}. In the quasi-neutral bulk of the n-Si, a standard mesh size of 500 nm and 5 μm was used transverse and parallel to the junction, respectively. Near the ohmic contact

with n-Si, the mesh was refined to 500 nm and 100 nm, and near the junction, the mesh was refined to 500 nm and 20 nm, to accurately model band-bending in these regions. The *J*-*E* (current vs. potential) characteristics of this structure were obtained by first solving for the $V = 0$ case in the dark. Subsequently, the voltage was stepped at 0.01 V intervals in both the positive and negative directions, to obtain the dark *J*-*E* behavior. The carrier generation rate from Lumerical was then applied to extract the *J*-*E* characteristics in the presence of illumination. Similarly, the $V = 0$ case in the light was solved first, and then the voltage was stepped at 0.01 V intervals, to obtain the light *J*-*E* performance. Shockley-Reed-Hall recombination was used for all simulations.

[00116] ***WO_3-liquid junction.*** The built-in "oxide as semiconductor" materials parameter file was used to model WO_3, with the following parameters and their values in parentheses: modified band-gap ($E_g = 2.6$ eV), work function ($\chi = 4.4$ eV), relative permittivity ($\epsilon_r = 5.76$), conduction- and valence-band density of states ($N_C = 1.8 \times 10^{19}$ cm^{-3}, $N_V = 7.1 \times 10^{19}$ cm^{-3}), time constant ($\tau_n = \tau_p = 1 \times 10^{-8}$ s) and mobility ($\mu_n = \mu_p = 40$ cm^2 V^{-1} s^{-1}). The band-gap was experimentally measured from absorption measurements using an integrating sphere and a Tauc plot. The relative permittivity was calculated from ellipsometric measurements of the complex refractive index. The work function was chosen based on reports found in the literature. The density of states can be calculated from m^*, the effective mass of holes in the valence band and of electrons in the conduction band (Equation 3):

$$N_c = 2\left(\frac{2\pi m_e^* k_B T}{h^2}\right)^{3/2} \quad (3)$$

Effective masses in the conduction band have been reported to be ~ 0.8 m_0, where m_0 is the mass of a free electron. Density functional theory calculations of the band structure of WO_3 indicate that the valence band has less curvature than the conduction band, indicating heavier holes and leading to an estimate of 2 m_0 for the hole effective mass. The mobility values were also taken from the

literature. Preliminary experimental measurements indicated a diffusion length of 1 μm, thereby determining the time constant.

[00117] The WO_3/liquid junction was modeled as a Schottky junction, with the metal work function equal to the water oxidation redox potential, χ = 5.68 eV, which was in contact with a 1 μm thick slab of WO_3. A value of $N_D = 10^{15}$ cm^{-3} was chosen to match the experimentally observed short-circuit current density and open-circuit voltage. Mesh sizes of 10 nm and 250 nm were used perpendicular and parallel to the junction, respectively. The method to obtain the dark and light *J-E* behavior was identical to that used for modeling the Si junction. Shockley-Reed-Hall recombination and thermionic emission physics were used for these simulations.

[00118] **Hydrogen Evolution Catalysis Modeling.** Butler-Volmer kinetics in the absence of mass transport limitations were used with $\alpha = 1$ and $j_0 = 10^{-3}$ A-cm^{-2}, to simulate the cathodic overpotential (Equation 4) of platinum (Pt) for hydrogen evolution in 1.0 M H_2SO_4.

$$\eta = -\frac{RT}{F}\ln\left(\frac{J}{J_0}+1\right) \quad (4)$$

[00119] The overpotential was added to the n-p^+-Si homo-junction *J-E* data at the same current density to yield a simulated hydrogen generation device curve in the absence of mass transport.

[00120] Light absorption modeling was carried out via full-field (E,H) electromagnetic simulations in a commercial software package, Lumerical FDTD. Simulations were performed at discrete wavelengths, ranging from 350nm to 1100nm at 50nm intervals, to capture absorption distributions up to the band edge of silicon. Discrete wavelength simulations have been shown to outperform broadband simulations. The light absorption in each material was calculated from the spatially resolved electric field data. Light absorption at each wavelength was then weighted by the AM1.5G spectrum to obtain an ideal short circuit current density, assuming unity internal quantum efficiency (IQE). The ideal short circuit current density is the main figure of merit used to evaluate the efficiency of light absorption.

[00121] To illustrate the effect of both geometry and material selection on light absorption in a PEC device, two disparate optoelectronic designs (Figure 2) were explored. The main difference between the two designs is in the optical properties of their contact materials (transparent contact=indium tin oxide (ITO); opaque contact=aluminum (Al)), which motivates different electronic designs.

[00122] The aim of the opaque contact design is to enable multiple photon path lengths through the photoanode, which in the case of WO_3 (E_g=2.6eV) and other wide bandgap oxides, is the current-limiting material ($J_{sc,ideal}$,WO_3=4mA/cm^2 under AM1.5G illumination). As an indirect bandgap material, WO_3 greatly benefits from multiple photon path lengths because its optical thickness is ~100μm near the band edge. The disadvantage of this design is that the opaque contact layer absorbs a significant portion of the light due to surface plasmon absorption.

[00123] The standard dimensions for the core/shell Z-scheme model are 7μm pitch arrays of 100μm tall silicon microwires with 1μm radii; the top 50μm of the wires are conformally coated with 100nm of a contact material and 1μm of WO_3. The initial shape of the WO_3, was chosen as the most likely experimental deposition shape. Many variations on these specifications have been explored.

[00124] An optically-thick planar aluminum substrate absorbs 7% and reflects 93% of incoming light at normal incidence, which enables multiple photon path lengths through the WO_3 via reflection to maximize its absorption. A plot of the fraction of light absorbed by each material versus wavelength is shown in Figure 8. The aluminum absorbed much more than 7% of the incident light in this design, peaking at around 50% absorption at 850nm, and amounting to a total of 15.22mA/cm^2.

[00125] Investigation of absorption with angle dependence, multiple structural shapes of WO_3 and Al (Figure 9), and different opaque contact materials (*e.g.* silver) showed that the lossy contact absorption persists when the contact material is opaque across the UV and visible spectrum. These results are indicative of wave

guiding effects, including surface plasmon-polariton modes (SPPs), photonic modes, and scattering effects.

[00126] For aluminum in WO_3, the surface plasmon resonance is at λ=208nm, implying that the entire AM1.5G Spectrum can potentially couple into an SPP mode. The top edges of the wires enable coupling into a surface plasmon mode. Videos of the propagation of the electric field along the interface at different wavelengths elucidated the existence of an SPP mode at the aluminum interface. The speed of light was slower along the interface with respect to the free space wave, and the electric field decayed evanescently away from the surface. Based on these observations, an SPP mode definitely contributes to the excessive absorption in the aluminum layer. Additionally, the significant enhancement of the aluminum absorption in the wire structure over the planar case (Figure 10) supports the claim of an SPP mode, which can only be coupled into with the assistance of the wire edges.

[00127] Additional waveguiding effects are clearly present due to the silicon wire array geometry. Photonic modes and scattering effects also help account for absorption exceeding that of a planar substrate. Photonic modes are an embodiment of light trapping due to a high index material, which is the case for WO_3 and also for aluminum around 800nm.

[00128] The transparent model is of interest due to the major absorption losses associated with the opaque model. The transparent contact incites a decrease in the WO_3 current from $1mA/cm^2$ (the opaque contact) to $0.7mA/cm^2$ because photons only have a single path length through the photoanode material before passing into the photocathode.

[00129] To make a transparent contact a viable option for the Si/WO_3 system, the WO_3 absorption must be increased. One approach is to increase the amount of WO_3 material in the design; however, tentative experimental values for the diffusion length are around 1μm, indicating that increasing the material width to 2μm may not significantly increase the collected current. However, the synthesis of porous

[00130] WO_3 may remedy this issue; measurements of the diffusion length of porous WO_3, revealed effective diffusion lengths of 40um. These issues are investigated further with carrier transport modeling. Light absorption in WO_3 doubles using a design such as model G (Figure 9) with an ITO contact, resulting in a short circuit current of 1.44mA/cm^2. The main losses in this model are in transmission and reflection, which, unlike contact absorption losses, have simple and thoroughly studied solutions, namely an antireflective coating and a back reflector.

[00131] Further optimization of this model was investigated via the incorporation of an AR coating. The optimum index for an AR coating is the square root of the index of the material to be coated. The refractive index of WO_3 within its band edge is 2.4, making silicon dioxide (SiO_2), with an index of 1.45, a fairly good match. Therefore, a 100nm coating of SiO_2 was added to the top of the WO_3. Consequently, reflection losses decreased, and the WO_3 current rose to 1.55mA/cm^2. The addition of a back reflector (and no AR coating) affected an increase in the WO_3 current to 1.97mA/cm^2, by eliminating transmission losses.

[00132] Because the back reflector directs light back into the silicon and subsequently the WO_3, the majority of the current gain is observed in the silicon. To decrease transmission in a way that benefits the photoanode preferentially over the photocathode, the pitch can be decreased. With a pitch of 5um, the WO_3 current increases to 1.97mA/cm^2, and the transmission drops to 1.78mA/cm^2. It is important to note that this method decreases the void fraction (and thus, increases the material volume), and therefore will increase the material cost for such a device. Material cost is probably not an issue for silicon and WO_3.

[00133] When all three of these optimization techniques are combined (AR coating, back reflector, and smaller pitch), the WO_3 current reaches 2.1mA/cm^2, which is double that of the original model and achieves 50% of its possible short-circuit current density (4mA/cm^2). Employing these same three changes in the opaque contact design results in a comparable WO_3 current of 2.03mA/cm^2, but reduces the silicon absorption to 0.16mA/cm^2. This comparison illustrates

the concept that the transparent contact losses are rectifiable while the opaque design losses are not. The remaining losses in the transparent contact design are from reflection and incomplete absorption in the WO_3 that is subsequently absorbed by the silicon.

[00134] The study of light absorption in the opaque contact design revealed that reflection could be greatly decreased by changing the round morphology of the top of the WO_3 to a flat surface (Model A, Figure 9). When this strategy is applied to the transparent contact design discussed above, the WO_3 current increases from 2.1mA/cm^2 to 2.56mA/cm^2. This gain is actually due to the elimination of the focusing effect that is created by the round top. With a flat top, more of the light is directed straight down into the WO_3 instead of towards the silicon.

[00135] Another means to decrease the losses to silicon is to increase the WO_3 thickness. The limit on the effectiveness of this strategy will be determined by carrier transport properties. By increasing the height of the top of the WO_3 to 2μm, the ideal short circuit current increased to 2.6mA/cm^2. This is not a significant gain considering that a portion of it will not be collected due to carrier transport limitations.

[00136] Another option is to incorporate a highly reflective (HR) coating between the WO_3 and silicon to reflect light back into the WO_3 and regain the multiple photon path lengths that were accessible in the opaque contact design. Ideally, a transparent contact material could serve this purpose, as well, with the proper index. The reflection, *R*, at an interface can be calculated from the following equation, where n_1 and n_2 are the refractive indices of the first and second media, respectively:

$$R = \left(\frac{n_1 - n_2}{n_1 + n_2}\right)^2$$

[00137] Within the band edge of WO_3, the refractive indices of WO_3 and silicon are roughly 2.4 and 5.6, respectively. The interface between WO_3 and silicon reflects 16% of the light back into the WO_3. If a layer of SiO_2 is placed between the WO_3 and the silicon, then 7% will be reflected back into the WO3 at the WO_3/SiO_2 interface and 36%

of the light reaching the SiO_2/Si interface will be reflected back toward the WO_3; ultimately, a SiO_2 layer would theoretically increase reflection back into the WO_3 layer by about 25%. For modeling purposes, a 100nm coating of a dielectric material with a refractive index of 1.5 was used in place of the ITO. This HR coating increased the WO_3 current to 2.65mA/cm^2.

[00138] For the case of a current-limiting photocathode, the reverse of this strategy should be used. These results reveal that tuning the index of the photoelectrode interfacial material is a more effective means to increase light absorption in a given material than simply increasing material thickness. In fact, index tuning is also more favorable when carrier transport is taken into account, assuming that a low index, electrically-conductive alternative to SiO_2 can be used.

[00139] Accordingly, an optimized structure for the transparent contact design is a 5μm pitch array of spearshaped silicon wires, coated conformally with 100nm of a transparent contact material with a refractive index in the range of 1.4 to 1.6, subsequently coated in 1μm of WO_3, which has a flat top coated in 100nm of SiO_2, all on top of a back reflector.

[00140] Although a number of embodiments and features have been described above, it will be understood by those skilled in the art that modifications and variations of the described embodiments and features may be made without departing from the teachings of the disclosure or the scope of the invention as defined by the appended claims.

WHAT IS CLAIMED IS:

1. An elongated structure comprising a plurality of radially-integrated tandem junctions separated by a transparent low resistance layer, wherein a first junction comprising a first semiconductive material and at least a second junction comprises a second different or the same semiconducting material having a different or the same band gap compared to the first semiconductive material.

2. The elongated structure of claim 1, wherein the first junction and second junction are separated by a low resistance layer comprising a transparent conductive oxide.

3. The elongated structure of claim 1 or 2, wherein the low resistance layer comprise a material selected from the group consisting of TiO_2, $CaTiO_3$, $SrTiO_3$, $Sr_3Ti_2O_7$, $Sr_4Ti_3O_{10}$, $Rb_2La_2Ti_3O_{10}$, $Cs_2La_2Ti_3O_{10}$, $CsLa_2Ti_2NbO_{10}$, La_2TiO_5, $La_2Ti_3O_9$, $La_2Ti_2O_7$, $La_2Ti_2O_7$:Ba, $KaLaZr_{0.3}Ti_{0.7}O_4$, $La_4CaTi_5O_{17}$, $KTiNbO_5$, $Na_2Ti_6O_{13}$, $BaTi_4O_9$, $Gd_2Ti_2O_7$, $Y_2Ti_2O_7$, ZrO_2, $K_4Nb_6O_{17}$, $Rb_4Nb_6O_{17}$, $Ca_2Nb_2O_7$, $Sr_2Nb_2O_7$, $Ba_5Nb_4O_{15}$, $NaCa_2Nb_3O_{10}$, $ZnNb_2O_6$, $Cs_2Nb_4O_{11}$, La_3NbO_7, Ta_2O_5, $KsPrTa_5O_{15}$, $K_3Ta_3Si_2O_{13}$, $K_3Ta_3B_2O_{12}$, $LiTaO_3$, $KTaO_3$, $AgTaO_3$, $KTaO_3$:Zr, $NaTaO_3$:La, $NaTaO_3$:Sr, $Na_2Ta_2O_6$, $CaTa_2O_6$, $SrTa_2O_6$, $NiTa_2O_6$, $Rb_4Ta_6O_{17}$, $Ca_2Ta_2O_7$, $Sr_2Ta_2O_7$. $K_2SrTa_2O_7$, $RbNdTa_2O_7$, $H_2La_{2/3}Ta_2O_7$, $K_2Sr_{1.5}Ta_3O_{10}$, $LiCa_2Ta_3O_{10}$, $KBa_2Ta_3O_{10}$, $Sr_5Ta_4O_{15}$, $Ba_2Ta_4O_{15}$, $H_{1.8}Sr_{0.81}Bi_{0.19}Ta_2O_7$, Mg—Ta Oxide, $LaTaO_4$, $LaTaO_7$, $PbWO_4$, $RbWNbO_6$, $RbWTaO_6$, CeO_2:Sr, $BaCeO_3$, $NaInO_2$, $CaIn_2O_4$, $SrIn_2O_4$, $LaInO_3$, $Y_xIn_{2-x}O_3$, $NaSbO_3$, $CaSb_2O_6$, $Ca_2Sb_2O_7$, $Sr_2Sb_2O_7$, Sr_2SnO_4, $ZnGa_2O_4$, Zn_2GeO_4, $LiInGeO_4$, Ga_2O_3[b], Ga_2O_3:Zn[c],$Na_2Ti_3O_7$, $K_2Ti_2O_5$, $K_2Ti_4O_9$, $Cs_2Ti_2O_5$, H^+-$Cs_2Ti_2O_5$, $Cs_2Ti_5O_{11}$, $Cs_2Ti_6O_{13}$, H^+-$CsTiNbO_5$, H^+-$CsTi_2NbO_7$, SiO_2-pillared $K_2Ti_4O_9$, SiO_2-pillared $K_2Ti_{2.7}Mn_{0.3}O_7$, $Na_2W_4O_{13}$, H^+-$KLaNb_2O_7$, H^+-$RbLaNb_2O_7$, H^+-$CsLaNb_2O_7$, H^+-$KCa_2Nb_3O_{10}$, SiO_2-pillared $KCa_2Nb_3O_{10}$, ex-$Ca_2Nb_3O_{10}/K^+$ nanosheet[4)], Restacked ex-$Ca_2Nb_3O_{10}/Na^+$, H^+-$RbCa_2Nb_3O_{10}$, H^+-$CsCa_2Nb_3O_{10}$, H^+-$KSr_2Nb_3O_{10}$, H^+-$KCa_2NaNb_4O_{13}$. $Bi_2W_2O_9$, $Bi_2Mo_2O_9$, $Bi_4Ti_3O_{12}$, $BaBi_4Ti_4O_{15}$, Bi_3TiNbO_9, $PbMoO_4$, $(NaBi)_{0.5}MoO_4$, $(AgBi)_{0.5}MoO_4$, $(NaBi)_{0.5}WO_4$, $(AgBi)_{0.5}WO_4$, $Ga_{1.14}In_{0.86}O_3$, β-Ga_2O_3, $Ti_{1.5}Zr_{1.5}(PO_4)_4$, WO_3, Bi_2WO_6, Bi_2MoO_6, $Bi_2Mo_3O_{12}$, $Zn_3V_2O_8$, $Na_{0.5}Bi_{1.5}VMoO_8$, $In_2O_3(ZnO)_3$, $SrTiO_3$:Cr/Sb, $SrTiO_3$:Ni/Ta, $SrTiO_3$:Cr/Ta, $SrTiO_3$:Rh, $CaTiO_3$:Rh, $La_2Ti_2O_7$:Cr, $La_2Ti_2O_7$:Fe, TiO_2:Cr/Sb, TiO_2:Ni/Nb, TiO_2:Rh/Sb,

$PbMoO_4$:Cr, $RbPb_2Nb_3O_{10}$, $PbBi_2Nb_2O_9$, $BiVO_4$, $BiCu_2VO_6$, $BiZn_2VO_6$, $SnNb_2O_6$, $AgNbO_3$, Ag_3VO_4, $AgLi_{1/3}Ti_{2/3}O_2$, $AgLi_{1/3}Sn_{2/3}O_2$, $LaTiO_2N$, $Ca_{0.25}La_{0.75}TiO_{2.25}N_{0.75}$, TaON, Ta_3N_5, $CaNbO_2N$, $CaTaO_2N$, $SrTaO_2N$, $BaTaO_2N$, $LaTaO_2N$, $Y_2Ta_2O_5N_2$, $TiN_xO_yF_z$, $Sm_2Ti_2O_5S_2$, La-In oxysulfide, GaAs, GaP, $GaAs_xP_{1-x}$, Al_xGa_{1-x}, As, $Al_xGa_{1-x}As_yP_{1-y}$, $In_xGa_{1-x}As$, $In_xGa_{1-x}P$, $In_xGa_{1-x}As_yP_{1-y}$, $Al_xIn_{1-x}As_yP_{1-y}$, $Al_xGa_{1-x}As_yN_zP_{1-y-z}$, $In_xGa_{1-x}As_yN_zP_{1-y-z}$, Zn_3P_2, Zn_3S_2, and ZnP_xS_{1-x} ($0 \le x \le 1$, $0 \le y \le 1$, $0 \le z \le 1$, $0 \le y+z \le 1$).

4. The elongated structure of claim 1 or 2, wherein the second semiconductive layer comprises a material selected from the group consisting of GaAs, GaP, $GaAs_xP_{1-x}$, Al_xGa_{1-x}, As, $Al_xGa_{1-x}As_yP_{1-y}$, $In_xGa_{1-x}As$, $In_xGa_{1-x}P$, $In_xGa_{1-x}As_yP_{1-y}$, $Al_xIn_{1-x}As_yP_{1-y}$, $Al_xGa_{1-x}As_yN_zP_{1-y-z}$, $In_xGa_{1-x}As_yN_zP_{1-y-z}$, Zn_3P_2, Zn_3S_2, and ZnP_xS_{1-x} ($0 \le x \le 1$, $0 \le y \le 1$, $0 \le z \le 1$, $0 \le y+z \le 1$).

5. The elongated structure of claim 1 or 2, wherein the low resistance layer comprises indium tin oxide (ITO).

6. The elongated structure of any one of claims 1-5, wherein the elongated structure has a dimension comprising 500 nm to about 10 micrometers in diameter and about 1 micrometer to 1 mm in length or wherein the elongated structure has a mean diameter less than 1 micrometer and a length of less than 1 micrometer and an aspect ratio of greater than 1.

7. The elongated structure of any one of the foregoing claims wherein the elongated structure has an aspect ratio greater than 1.

8. The elongated structure of any one of the foregoing claims, wherein the first semiconductive material is Si.

9. The elongated structure of any one of the foregoing claims, wherein the elongated structure is substantially embedded in a material selected from the group consisting of glass, polymer and wax.

10. The elongated structure of claim 9, wherein the material forms a membrane comprising the elongated structure embedded in the material extending from and/or through a first surface to and/or through a second surface of the membrane.

11. The elongated structure of any one of the foregoing claims, wherein one or both ends of the elongated structure are coated with a catalyst.

12. The elongated structure of any one of the foregoing claims wherein the tops of the wires are flat.

13. The elongated structure of claim 1, wherein:

the first semiconductive layer comprises a material selected from the group consisting of crystalline Si, multicrystalline Si, GaAs, InP, CdTe and alloys of any of the foregoing, or group IV metal dichalcogenides;

the low resistance layer comprise a material selected from the group consisting of ITO (In-SnO_2), FTO (F-doped SnO_2), and TiO_2; and

the second semiconductive layer comprises a material selected from the group consisting of WO_3, BiVO4, Fe_2O_3, GaP, CdSe, and amorphous-Si.

14. The elongated structure of claim 13, wherein the group IV metal dicholcogenides is selected from the group consisting of MoS_2, WS_2, $MoSe_2$, and WSe_2.

15. A method of making an elongated structure of claim 1, comprising:

(a) fabricating a first semiconductive structures on a Si substrate comprising

(i) forming a templated oxide layer on the substrate, wherein the template for the templated oxide layer comprises openings in the oxide layer for the formation of a first semiconductive structure; and

(ii) growing a set of first semiconductive structures on the substrate, wherein the first semiconductive structure growth is supported by a catalyst deposited in the openings in the oxide layer;

(b) coating the fabricated first semiconductive structures in an oppositely doped semiconductive material layer to generate an emitter layer;

(c) coating the emitter layer with an transparent low resistance layer; and

(d) radially and epitaxially applying a second semiconductive material on the transparent low resistance layer, wherein the second semiconductive material has the same or wider band-gap as the first semiconductive material.

16. The method of claim 15, wherein the low resistance layer comprises a semiconductive material.

17. The method of claim 15, wherein the low resistance layer comprises a transparent conductive oxide.

18. The method of claim 17, wherein the transparent conductive oxide is selected from the group consisting of cadmium tin oxide (CTO), indium tin oxide (ITO), fluorine-doped tin oxide (SnO:F or FTO), indium-doped cadmium-oxide, cadmium stannate (Cd_2SnO_4 or CTO), doped zinc oxide (ZnO), such as aluminum-doped zinc-oxide (ZnO:Al or AZO), indium-zinc oxide (IZO), zinc tin oxide ($ZnSnO_x$), and combinations thereof.

19. The method of any one of claims 15-18, wherein the elongated structure is substantially embedded in a wax, glass or polymer.

20. The method of claim 19, wherein the embedded elongated structure are mechanically removed from the Si substrate.

21. The method of claim 15, further comprising applying a hydrogen evolving and/or oxygen evolving catalyst to the elongated structure.

22. The method according to claim 21, wherein the catalyst is selected from the group consisting of Pt, Co, Cu, Fe, MoS_x where x is nominally 2, or a sub or super-stoichiometric, Ni, CoMo, CoW, FeMo, NiCo, NiFe, NiFeC, NiFeS, NiMnS, NiMo, NiMoP, NiSn, NiW, NiZn, NiZnP, CoNiFe, NiCoPMo, NiMoCo, NiMoCu, NiMoFe, NiMoW, NiSiMo, NiSiW, NiWPCu, IrO_x where x is nominally 2, or sub or super-stoichiometric, Pt, Co, $Co/(PO_4)^{3-}$, $Co/(BO_3)^{3-}$, CoP, Cu, Fe, Mn, Ni, $Ni/(BO_3)^{3-}$,NiP, Pb, CoFe, $CoPSc_2O_3$, FeMn, NiCo, NiCr, NiCu, NiFe, NiLa, NiLa, $NiPSc_2O_3$, NiSn, NiZn and NiMoFe.

23. A solar cell comprising the structure of any of claims 1-14.

24. A device or photocell comprising:

a substrate;

an ordered array of elongate semiconductor structures comprising at least 2 different semiconductive materials axially and radially integrated, wherein the elongate semiconductor structures have length dimensions defined by adjacent ends in electrical contact with at least portions of the substrate and distal ends not in contact with the substrate and have radial dimensions generally normal to the length dimensions and the radial dimensions are less than the length dimensions;

a transparent ohmic layer separating the at least 2 different semiconductive materials; and

wherein the device absorbs received light and converts it into electricity or chemical energy.

25. The device or photocell of claim 24, wherein the elongated semiconductor structures comprise wires.

26. The device or photocell of claim 25, wherein the elongate semiconductor structures are embedded in a matrix.

27. The device or photocell of claim 26, wherein the matrix is a glass, polymer or wax.

28. The device or photocell of claim 26 or 27, wherein the elongate semiconductor structures are partially or fully embedded in a matrix.

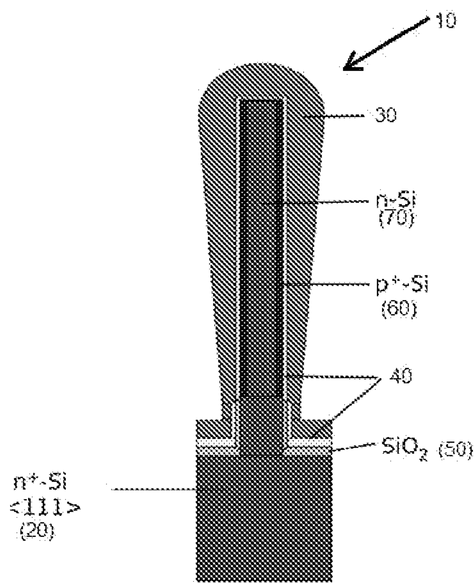

FIGURE 1A

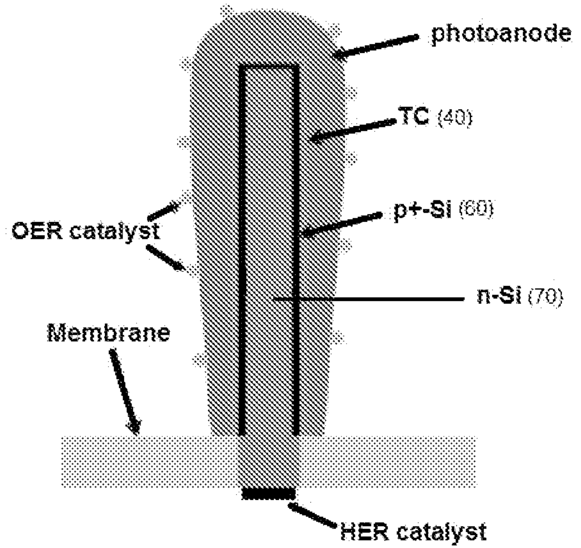

FIGURE 1B

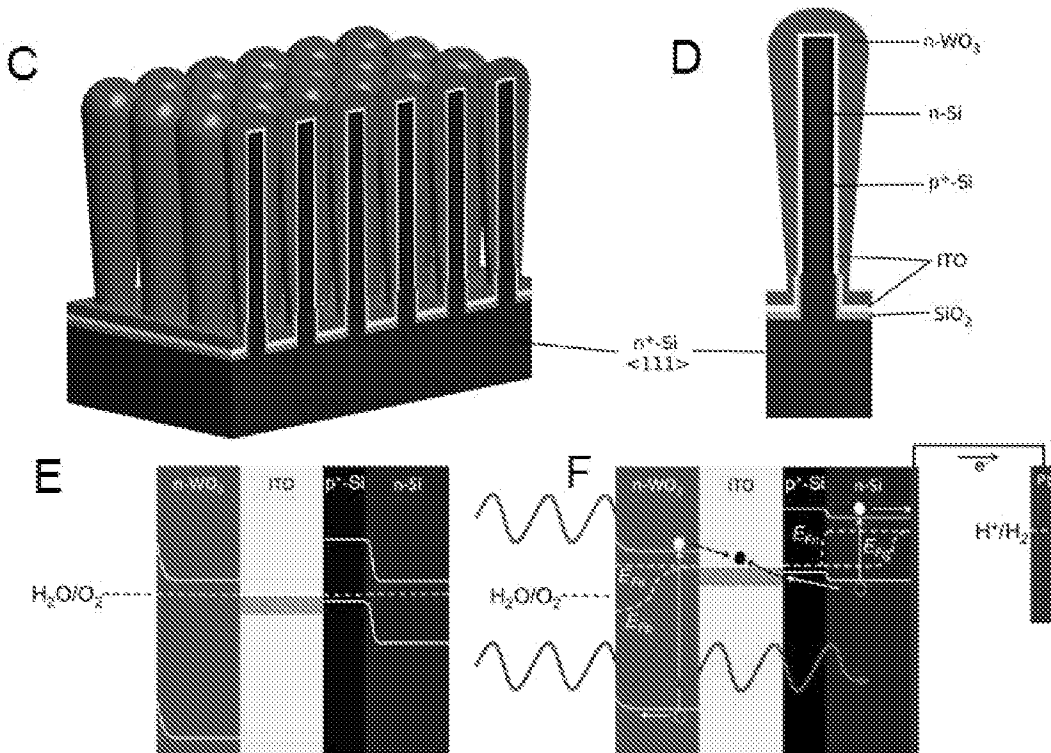

FIGURE 1B-F

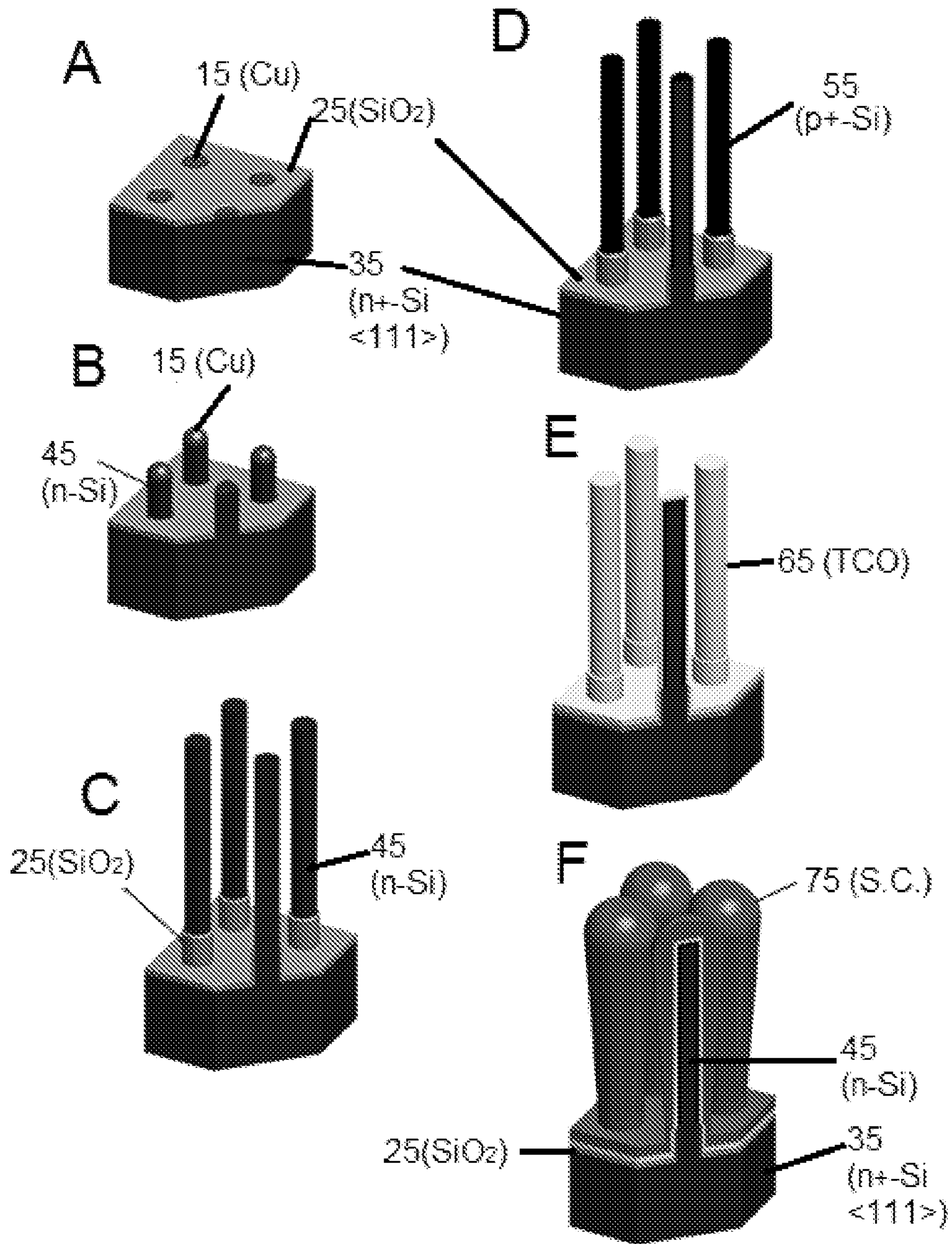

FIGURE 2A-F

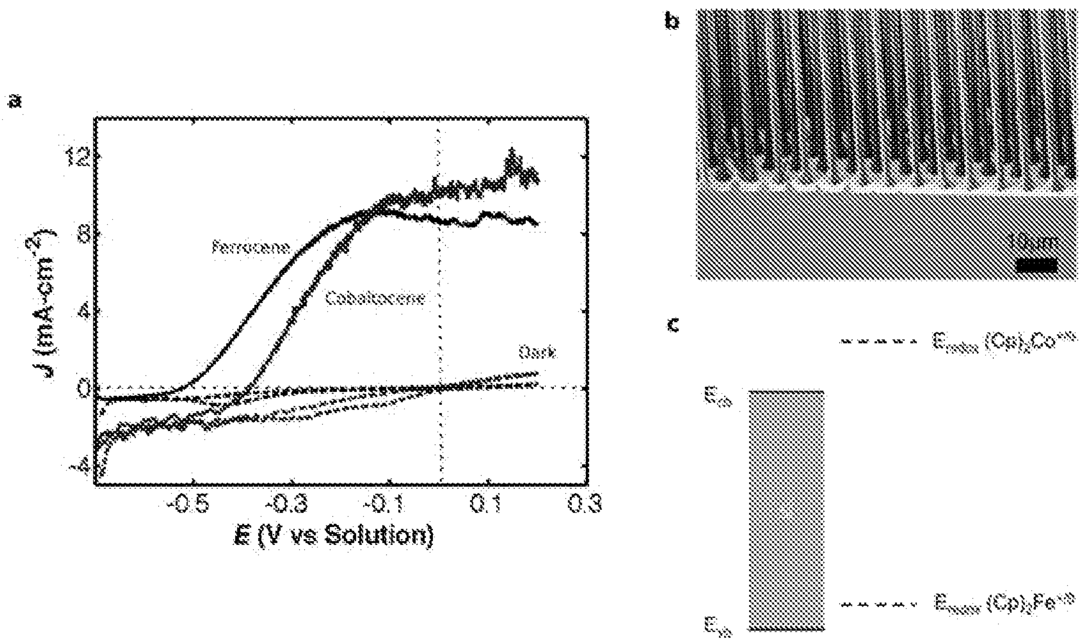

FIGURE 3A-C

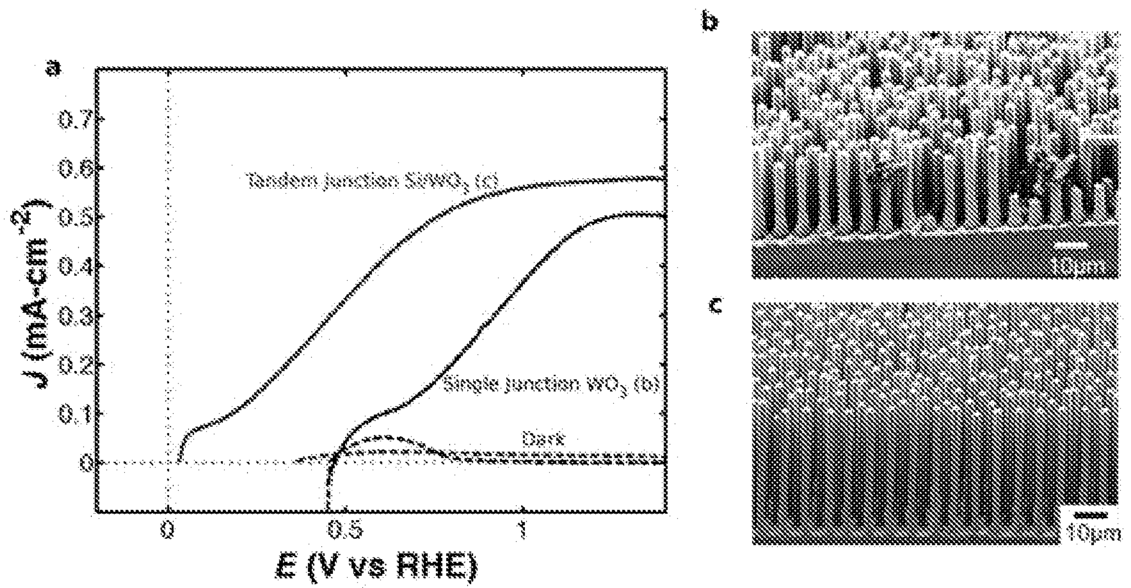

FIGURE 4A-C

4/9

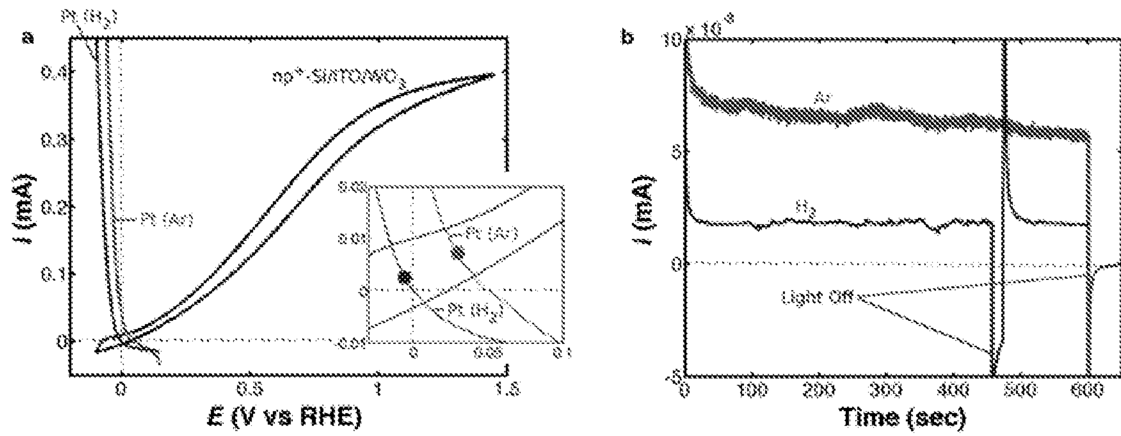

FIGURE 5A-B

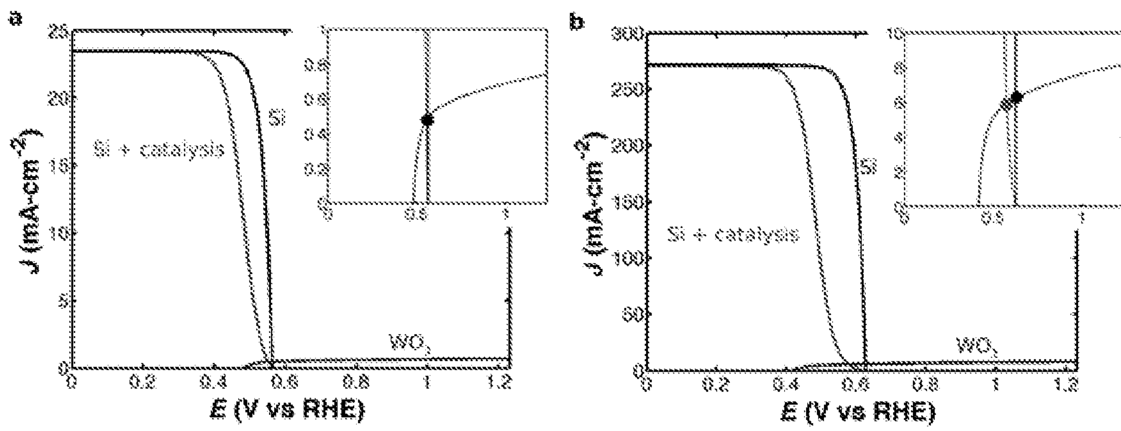

FIGURE 6A-B

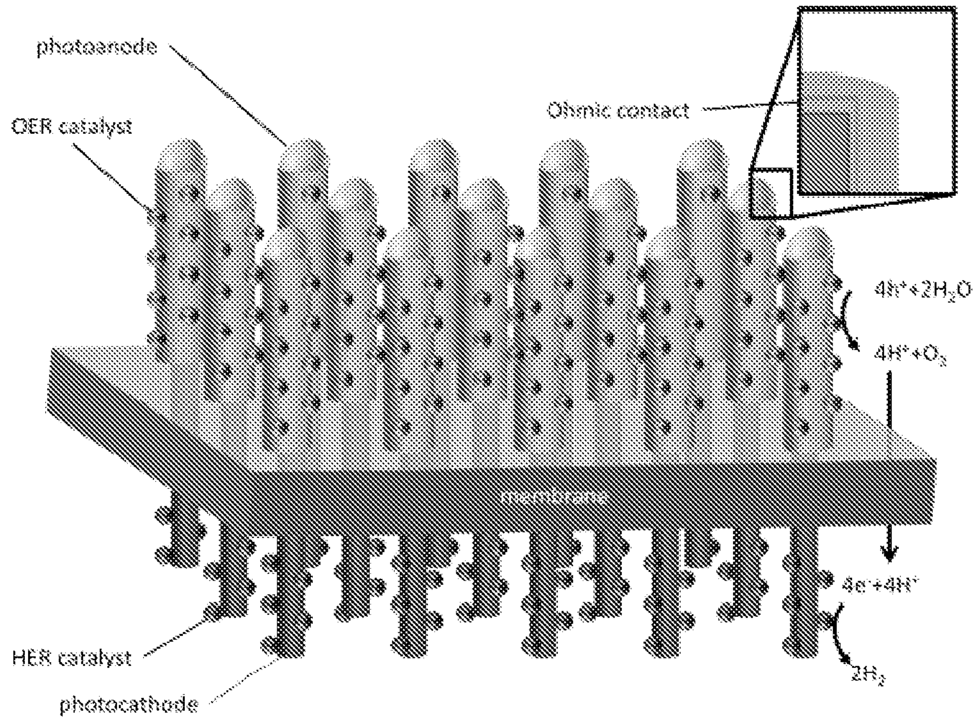

FIGURE 7

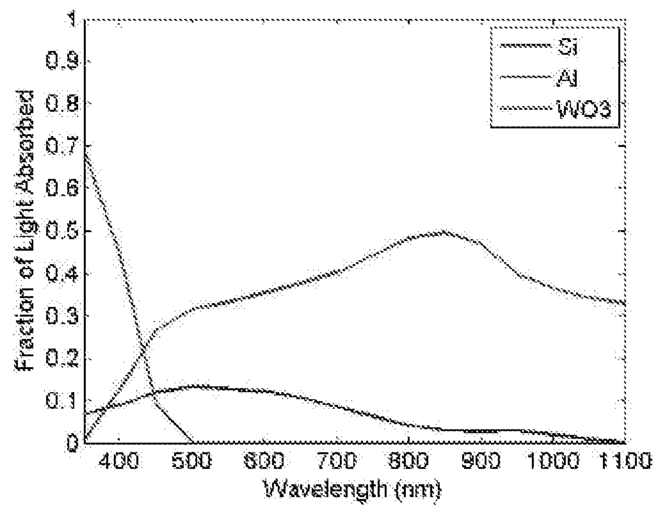

FIGURE 8

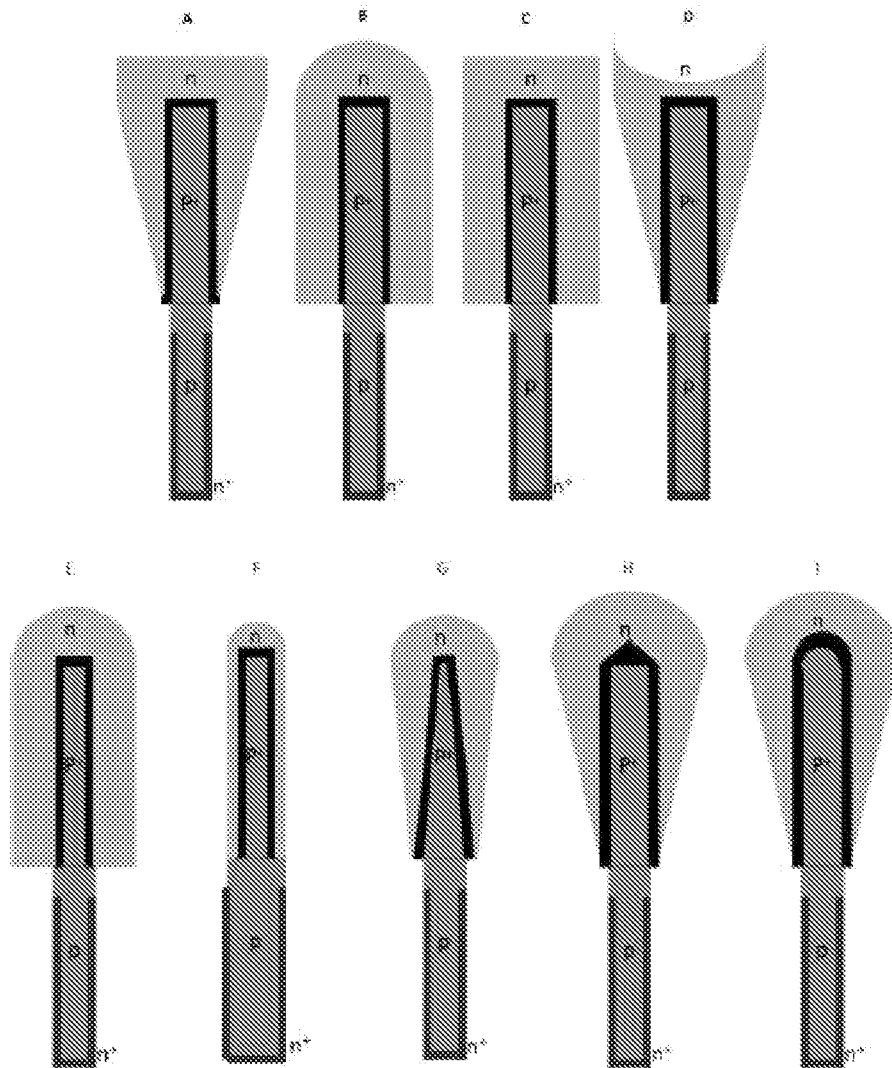

FIGURE 9A-I

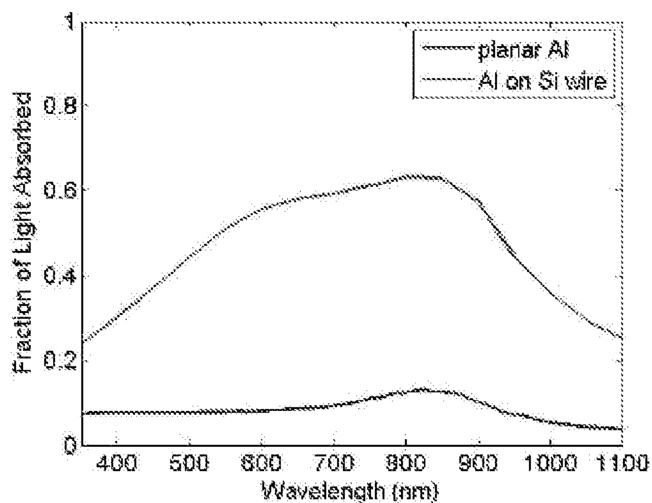

FIGURE 10

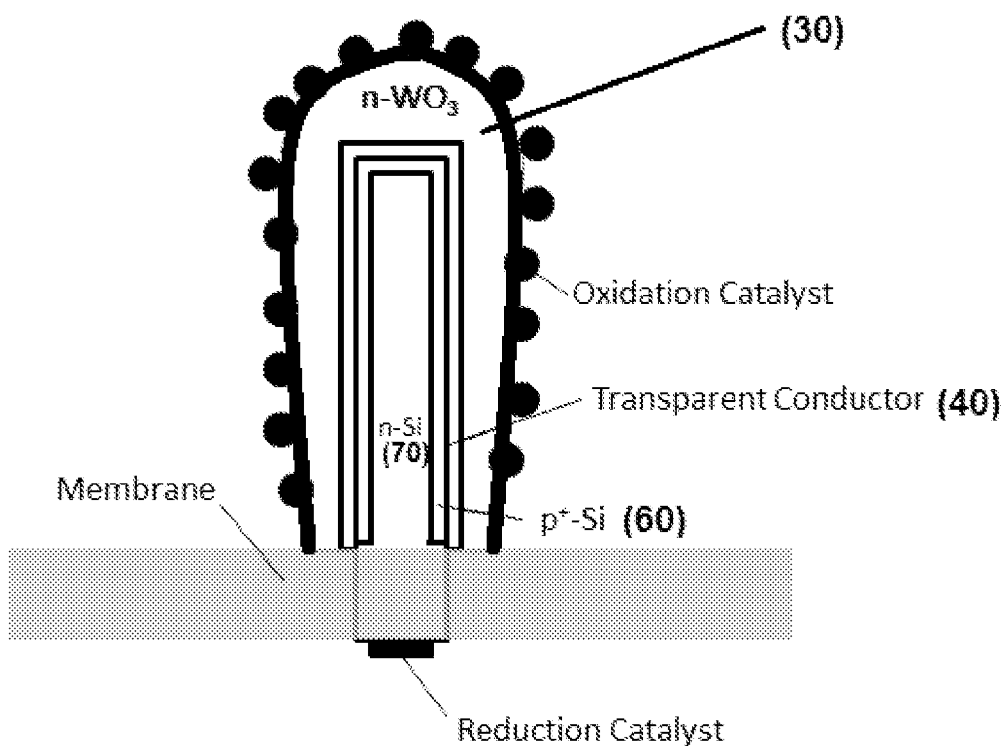

FIGURE 11A

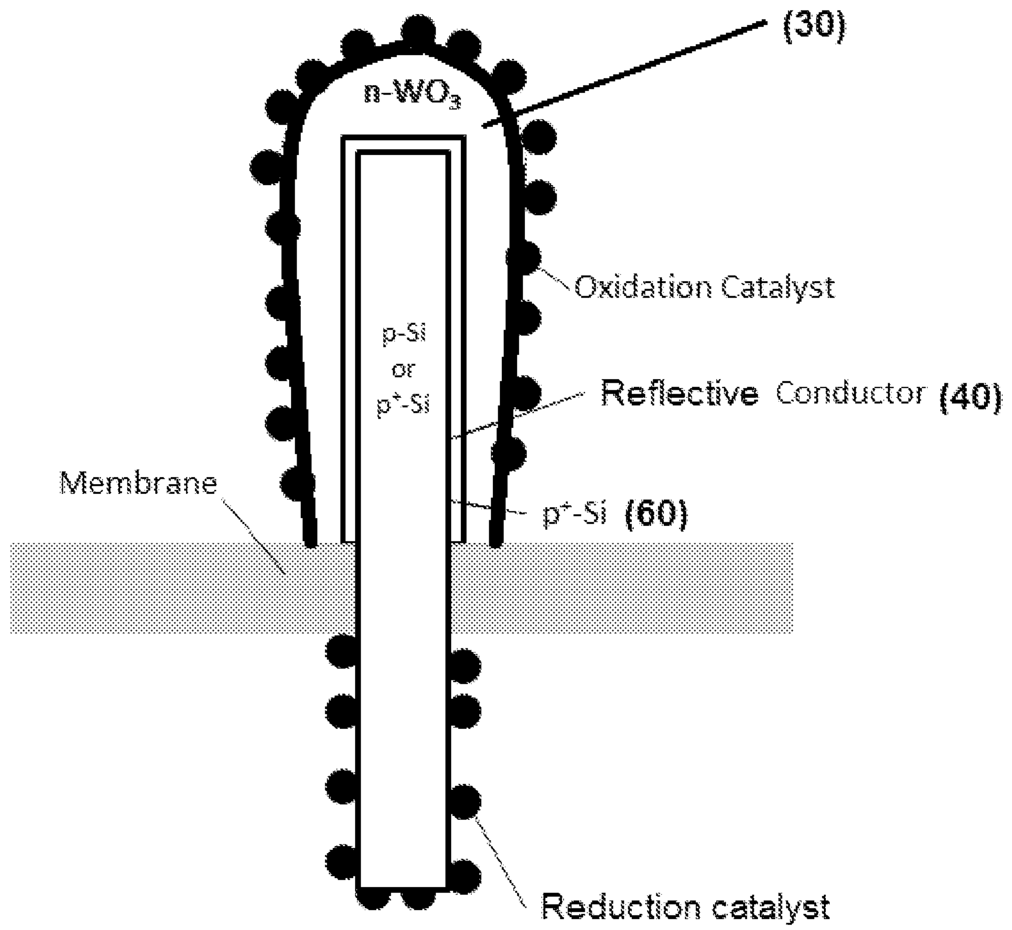

FIGURE 11B

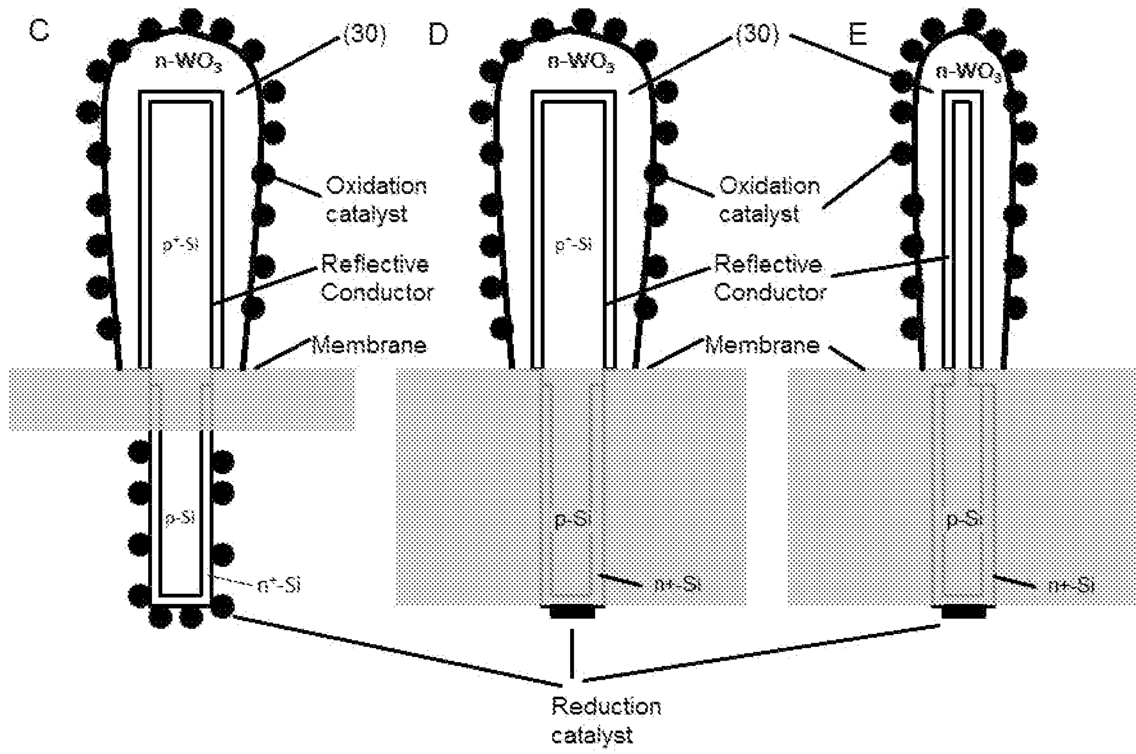

FIGURE 11 C-E

INTERNATIONAL SEARCH REPORT

International application No.
PCT/US2013/035171

A. CLASSIFICATION OF SUBJECT MATTER

H01L 31/042(2006.01)i, H01L 31/18(2006.01)i

According to International Patent Classification (IPC) or to both national classification and IPC

B. FIELDS SEARCHED

Minimum documentation searched (classification system followed by classification symbols)
H01L 31/042; H01L 31/02; H01L 31/06; B05D 1/36; H01L 31/0224; H01L 31/18; H01L 31/0352; H01L 31/04

Documentation searched other than minimum documentation to the extent that such documents are included in the fields searched
Korean utility models and applications for utility models
Japanese utility models and applications for utility models

Electronic data base consulted during the international search (name of data base and, where practicable, search terms used)
eKOMPASS(KIPO internal) & keywords: tandem junctions, photovoltaic, transparent, low resistance, band gap

C. DOCUMENTS CONSIDERED TO BE RELEVANT

Category*	Citation of document, with indication, where appropriate, of the relevant passages	Relevant to claim No.
X	US 2011-0269264 A1 (BASTIAAN ARIE KOREVAAR et al.) 03 November 2011 See paragraphs [0003]-[0009], [0056]-[0082]; and figures 1a-8.	1-28
A	US 2012-0006390 A1 (YIJIE HUO et al.) 12 January 2012 See paragraphs [0017]-[0026]; and figures 1a-3.	1-28
A	US 2011-0126891 A1 (HAJIME GOTO et al.) 02 June 2011 See paragraphs [0159]-[0262]; and figures 4-12.	1-28
A	US 2011-0139209 A1 (CHRISTIAN LANG et al.) 16 June 2011 See paragraphs [0122]-[0166]; and figures 4(a)-15.	1-28
A	US 2012-0000525 A1 (DENNIS J. FLOOD) 05 January 2012 See paragraphs [0099]-[0109]; and figures 5-7.	1-28

Further documents are listed in the continuation of Box C.

See patent family annex.

* Special categories of cited documents:
"A" document defining the general state of the art which is not considered to be of particular relevance
"E" earlier application or patent but published on or after the international filing date
"L" document which may throw doubts on priority claim(s) or which is cited to establish the publication date of citation or other special reason (as specified)
"O" document referring to an oral disclosure, use, exhibition or other means
"P" document published prior to the international filing date but later than the priority date claimed
"T" later document published after the international filing date or priority date and not in conflict with the application but cited to understand the principle or theory underlying the invention
"X" document of particular relevance; the claimed invention cannot be considered novel or cannot be considered to involve an inventive step when the document is taken alone
"Y" document of particular relevance; the claimed invention cannot be considered to involve an inventive step when the document is combined with one or more other such documents,such combination being obvious to a person skilled in the art
"&" document member of the same patent family

Date of the actual completion of the international search	Date of mailing of the international search report
24 July 2013 (24.07.2013)	**24 July 2013 (24.07.2013)**

Name and mailing address of the ISA/KR

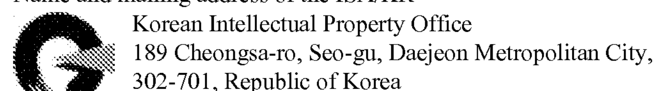
Korean Intellectual Property Office
189 Cheongsa-ro, Seo-gu, Daejeon Metropolitan City, 302-701, Republic of Korea
Facsimile No. +82-42-472-7140

Authorized officer
KIM Do Weon
Telephone No. +82-42-481-5560

INTERNATIONAL SEARCH REPORT

Information on patent family members

International application No.

PCT/US2013/035171

Patent document cited in search report	Publication date	Patent family member(s)	Publication date
US 2011-0269264 A1	03/11/2011	CN 101221993 A	16/07/2008
		CN 101221993 B	09/05/2012
		EP 1944812 A2	16/07/2008
		US 2008-169019 A1	17/07/2008
		US 8003883 B2	23/08/2011
		US 8435825 B2	07/05/2013
US 2012-0006390 A1	12/01/2012	None	
US 2011-0126891 A1	02/06/2011	JP 2011-135058 A	07/07/2011
US 2011-0139209 A1	16/06/2011	CN 102105963 A	22/06/2011
		EP 2319069 A1	11/05/2011
		EP 2319069 A4	09/01/2013
		GB 0813568 D0	03/09/2008
		GB 2462108 A	27/01/2010
		JP 2011-527096 A	20/10/2011
		WO 2010-010972 A1	28/01/2010
US 2012-0000525 A1	05/01/2012	CA 2723829 A1	13/11/2008
		US 2008-276987 A1	13/11/2008
		US 7999176 B2	16/08/2011
		WO 2008-137995 A1	13/11/2008